JOURNAL OF GUIDANCE, CONTROL, AND DYNAMICS
Vol. 34, No. 2, March–April 2011

Model-Free Control Design for Multi-Input Multi-Output Aeroelastic System Subject to External Disturbance

Z. Wang* and A. Behal†
University of Central Florida, Orlando, Florida 32826
and
P. Marzocca‡
Clarkson University, Potsdam, New York 13699

DOI: 10.2514/1.51403

In this paper, a class of aeroelastic systems with an unmodeled nonlinearity and external disturbance is considered. By using leading- and trailing-edge control surface actuations, a full-state feedforward/feedback controller is designed to suppress the aeroelastic vibrations of a nonlinear wing section subject to external disturbance. The full-state feedback control yields a uniformly ultimately bounded result for two-axis vibration suppression. With the restriction that only pitching and plunging displacements are measurable while their rates are not, a high-gain observer is used to modify the full-state feedback control design to an output feedback design. Simulation results demonstrate the efficacy of the multi-input multi-output control toward suppressing aeroelastic vibration and limit cycle oscillations occurring in pre and postflutter velocity regimes when the system is subjected to a variety of external disturbance signals. Comparisons are drawn with a previously designed adaptive multi-input multi-output controller.

Nomenclature

a	=	nondimensional distance from midchord to elastic axis
b, s	=	semichord, m, and wing section span, m
$C_{l\alpha}$, $C_{m\alpha}$	=	rate of change of lift, moment with respect to angle-of-attack, 1/rad
$C_{m\alpha-\text{eff}}$	=	rate of change of effective moment with respect to angle-of-attack, 1/rad
$C_{l\beta}$, $C_{m\beta}$	=	rate of change of lift, moment with respect to trailing-edge control surface deflections, 1/rad
$C_{m\beta-\text{eff}}$	=	rate of change of effective moment with respect to trailing-edge control surface deflections, 1/rad
$C_{l\gamma}$, $C_{m\gamma}$	=	rate of change of lift, moment with respect to leading-edge control surface deflections, 1/rad
$C_{m\gamma-\text{eff}}$	=	rate of change of effective moment with respect to leading-edge control surface deflections, 1/rad
c_h, c_α	=	structural damping coefficients in plunging, kg/s, and pitching, kg · m^2/s
$\mathbf{e}$, $\mathbf{r}$, $\mathbf{z}$	=	tracking error, filtered tracking error, and composite error
$\mathbf{F}$, $\mathbf{G}$, κ	=	neural network weight update gain matrices and constant
g_1, g_2	=	auxiliary saturation gains
$\mathbf{h}$, $\mathbf{f}$, $\mathbf{G_s}$, $\mathbf{T}$	=	system matrices
I_α	=	inertia of wing section about elastic axis, kg · m^2
$\mathbf{K}$, K_z	=	control gains
k_h, k_α	=	structural spring stiffness in plunging, N/m, and pitching N · m
L, M	=	aerodynamic lift, N, and moment, N · m
L_g, M_g	=	aerodynamic lift, N and moment, N · m, due to external disturbance
m_w, m_T	=	mass of wing and pitch-plunge system, kg
$\mathbf{N}$, $\hat{\mathbf{N}}$, $\mathbf{v}$	=	nonlinear target functions, neural networks compensator, and robustifying term
$\mathbf{S}$, $\mathbf{D}$, $\mathbf{U}$	=	factors of $\mathbf{G}_s$
t, τ	=	time variable, s and dimensionless time variable, $\tau = U_\infty t/b$
U_∞, ρ	=	freestream velocity, m/s, and air density, kg/m^3
$\mathbf{x}$, $\mathbf{u}$, $\mathbf{w}_{hd}$, $\mathbf{w}_g$	=	vector of system output, control input, and external disturbance terms
x_α	=	dimensionless distance from elastic axis to midchord
$\mathbf{W}$, $\mathbf{V}$	=	ideal neural networks weight matrices
$\hat{\mathbf{W}}$, $\hat{\mathbf{V}}$	=	estimated neural networks weight matrices
$\mathbf{Z}$, Z_B	=	ideal neural networks composite weight matrix and its bound
$\hat{\mathbf{Z}}$, $\tilde{\mathbf{Z}}$	=	estimated neural networks composite weight matrix and mismatch
α_1, a_2, $\bar{\epsilon}$	=	observer constants
α, h	=	pitching, rad, and plunging, m, displacements
β, γ	=	trailing-edge flap, rad, and leading-edge flap, rad, displacements
Λ, Φ, $\mathbf{\Pi}$, $\mathbf{\Psi}$	=	auxiliary signals and system vectors

Received 30 June 2010; revision received 10 October 2010; accepted for publication 19 October 2010.

*Graduate Student, Department of EECS.
†Assistant Professor, Department of EECS and NanoScience Technology Center.
‡Associate Professor, Mechanical and Aeronautical Engineering.

I. Introduction

THE development and implementation of passive and active feedback control capabilities in aerospace are current topics of research with many practical applications. In particular, active flutter suppression mechanisms are recently emerging as promising technologies aimed at providing solution for a large class of problems for aeronautical and aerospace flight vehicles that are prone to aeroelastic instabilities. Such instabilities can yield instantaneous catastrophic failure, e.g., flutter, or structural fatigue failure, due to persistent oscillations, e.g., limit cycle oscillations (LCOs) [1]. Dynamic aeroelastic effects may provide critical constraints on the flight vehicle performance, therefore, control strategies need to be implemented to safely perform maneuvers at the limit of the flight envelope. While aeroelastic instabilities can be postponed, providing an expansion of the flight envelope, by increasing the stiffness of the

wing, the byproduct of adding weight does decrease the overall performance of the flight vehicle. To the contrary, active suppression mechanisms lead to improved performance, and many control strategies have been applied to suppress flutter, divergence, control reversal, and detrimental wing oscillations. A possible vibration suppression mechanism can be implemented by feedback to control surfaces. A review of active control methods, wind-tunnel experiments, and flight experiences associated with feedback control and aeroelasticity was provided in [2]. A theoretical study of flutter suppression through full-state feedback with a Kalman estimator has been presented by Lyons et al. in [3]. Subsequently, more sophisticated higher-order models were developed. Mukhopadhyay et al. [4] developed a methodology for synthesizing optimal feedback control laws and applied them to active aeroelastic vibration suppression problems. Gangsaas et al. [5] provided practical gust load alleviation and flutter suppression control laws based on LQG methodology. In both control strategies, unmeasured states were described by estimators and output feedback was used as the control method. A partial-state feedback control law using pole placement technique was developed by Karpel [6] while Horikawa and Dowell [7] adopted proportional gain feedback methods, developed from root locus plots, to perform flutter suppression and load alleviation. The approach directly fed one of four variables to the control surface through a proportional gain. Flutter suppression has also been demonstrated experimentally. Heeg [8] has shown that the flutter velocity of a bending-torsion spring mounted small wing model can be increased by up to 20%. The control was somewhat simple but efficient, using root locus plots to derive proportional gain feedback control laws. By using a typical section with leading- and trailing-edge flaps, Lin [9] and Lazarus [10] demonstrated that a full-state feedback with an estimator was efficient as an active control mechanism. Experimental investigations were performed to demonstrate disturbance rejection, gust alleviation, and flutter suppression. Although these researchers have shown that linear control theory can be successfully applied, the need for more sophisticated aeroservoelastic models and control strategies stem from the fact that aircraft exhibit complex dynamical behaviors due to the presence of nonlinearities and more complex flight conditions.

Recently, there has been a significant increase in advancing methods to consider nonlinear aeroelasticity, especially, to account for the presence of softening or hardening structural stiffness effects and aerodynamic nonlinearities in the transonic or stall region. Dowell's book [11] sheds some light on the importance of considering nonlinearities in the aeroelastic analysis. Among the various nonlinearities, hardening structural nonlinearity, such as the one due to the presence of free play, gives rise to nonlinear stiffness, especially in torsion. Often this type of nonlinearity can have a pronounced effect, leading to a limited amplitude aeroelastic behavior, which is not catastrophic but may cause fatigue problems [12–16].

Several recent contributions related to the active control of aircraft wing exhibiting nonlinear behavior were discussed at length in [17]. In particular, some control strategies have been examined for a typical wing section with a single control surface and verified experimentally in [18–32] using traditional root locus and Nyquist method, linear quadratic Gaussian control, nonlinear control theory, feedback linearization techniques as well as robust and adaptive controllers. Generally, the pitching degree of freedom α was chosen as the primary output variable to regulate to zero amplitude. Initially, an adaptive cancellation of the nonlinearities introduced by the torsional stiffness led to a feedback linearized system; subsequently, a second control step aimed to enhance the aeroelastic response via conventional linear methods like LQR or pole placement where full-state feedback was usually adopted. In [28], control of the pitch angle trajectory using only output measurements was carried out using an adaptive backstepping design technique. Here, backstepping refers to a control design technique for a special class of nonlinear dynamical systems, a virtual control signal is designed initially to stabilize a system state, the error dynamics of the virtual controller (which can be construed as a virtual state) are stabilized using another virtual controller, and the process is continued recursively to stabilize the corresponding virtual states until reaching the external control which is finally designed. An adaptive control strategy was implemented in [29] using only the feedback for the pitching variable and its performance in subcritical flight speed range toward suppressing flutter and LCOs, as well as reducing the aeroelastic response in the subcritical flight speed regime was demonstrated. In [30], a robust control design for the global regulation of a two-degree-of-freedom (2-DOF) aeroelastic system was presented. The model had polynomial type structural nonlinearity and only the pitch angle was measured for feedback. It was also assumed that all the system parameters were unknown to the designer, but the bounds on uncertainties were known. A robust control strategy with the purpose of active flutter suppression of a nonlinear 2-D wing-flap system was presented [31]. An optimized robust stabilizer in the form of state feedback control and a proportional-integral observer (PI observer) was used as controller. The PI observer was used to estimate not only the system states but also the bounds of the nonlinearities present in the aeroelastic system. In [32], the adaptive control design problem for aeroelastic wing sections with structural nonlinearity was solved based on the immersion and invariance approach.

A novel way of improving the performance of the adaptive scheme via an extension to a wing section with two control surfaces was proposed in [33–36]. The scheme proposed in [33] was adaptive and used full-state feedback. However, the uncertainty in the coupling between the control inputs was not taken into account; instead, an inversion of the nominal input gain matrix was used to decouple the control inputs. In [34], adaptive and radial basis function neural network controllers were designed to compensate for the system nonlinearity and their performance was compared; a projection operator was used to assure that the input gain matrix estimate remained invertible. To sidestep the need for projection, an **ST** decomposition of the input gain matrix was used in [35] to design singularity free controllers for the leading- (LECS) and trailing-edge (TECS) control surfaces; this control design required full-state feedback as well as a filtered tracking error. Here, **S** is a symmetric, positive matrix and **T** is an upper triangular matrix with its diagonal elements belonging to the set $\{+1, -1\}$. In [36], an output feedback adaptive controller was designed using backstepping coupled with an **SDU** decomposition (symmetric-diagonal-upper triangular factorization). The aforementioned research work with two control surfaces was shown to have better dynamic performance than a single control surface. For details on backstepping design for multivariable systems using **SDU** factorization, the reader is referred to [37].

The adaptive control algorithms proposed previously in [29,35,36] are based on the assumption of linear-in-the-parameters models. However, the structure of the system nonlinearity may be unknown during the control design or it may not satisfy the linear-in-the-parameters assumption. Furthermore, various flow disturbances acting on the wing during flight (e.g., transient or sustained wind gusts) may not be easily modeled. Thus, the applicability and the robustness of adaptive control schemes to model errors cannot be guaranteed. Motivated by these practical questions when the system dynamics is unknown or partially available, our goal in this paper is to design an output feedback controller to suppress the flutter and LCOs for an unmodeled aeroelastic system subject to external disturbance. The two-flap active aeroelastic vibration suppression problem is formulated as an affine-in-the-control multi-input multi-output (MIMO) system with unstructured uncertainty; here, the input gain matrix is considered to be unknown, nonsymmetric with nonzero leading principal minors while the signs of its leading principal minors are assumed to be known for the purposes of control design. The problem is solved using an **SDU** decomposition to facilitate design of singularity-free leading- and trailing-edge controllers which is coupled with the design of model-free feedforward compensation and injected nonlinear robustification signals; specifically, a three-layer neural feedforward compensator is proposed in this paper. Through a Lyapunov analysis, it is shown that uniform ultimate boundedness (UUB) result can be obtained for tracking errors in the pitching and plunging variables. Furthermore, under the restriction that rates of pitching and plunging are not available for measurement, the full-state feedback control law is

modified to an output feedback result based on the design of a high-gain observer (HGO). Simulation results show that this control strategy can rapidly suppress the nonlinear aeroelastic flutter and oscillations. Compared with the adaptive backstepping results obtained in [36], the output feedback controller shows substantially greater robustness; here, robustness is defined as the ability of the controller to deal with uncertainty in the model and gust-type external disturbances. Saturation in the two control surfaces inputs is accounted for by the application of an antiwindup mechanism.

The rest of this paper is organized as follows. In Sec. II, the system dynamics are introduced. Then, the control objective is defined and the open-loop error system is developed to facilitate the subsequent control design. In Sec. III, the feedback and feedforward control design is proposed followed by a Lyapunov based analysis of stability of the closed-loop system. In Sec. IV, a solution based on a high-gain observer is proposed to design the output feedback controller. Simulation results to confirm the performance and robustness of the controller are presented in Sec. V. Concluding remarks are provided in Sec. VI.

II. Aeroelastic Model Configuration and Error System Development

A 2-DOF pitch-plunge wing section with both LECS and TECS is shown in Fig. 1 where both leading- and trailing-edge control surfaces are used as control inputs. The aeroelastic governing equation subject to external disturbance is developed from previous models in [16,33,38,39]:

$$\begin{bmatrix} m_T & m_w x_\alpha b \\ m_w x_\alpha b & I_\alpha \end{bmatrix}\begin{bmatrix} \ddot{h} \\ \ddot{\alpha} \end{bmatrix} + \begin{bmatrix} c_h & 0 \\ 0 & c_\alpha \end{bmatrix}\begin{bmatrix} \dot{h} \\ \dot{\alpha} \end{bmatrix} + \begin{bmatrix} k_h & 0 \\ 0 & k_\alpha(\alpha) \end{bmatrix}\begin{bmatrix} h \\ \alpha \end{bmatrix} = \begin{bmatrix} -L - L_g \\ M + M_g \end{bmatrix} \tag{1}$$

The definition of symbols used in above equation can be found in the nomenclature. In Eq. (1), the quasi-steady lift $L(\dot{h}, \dot{\alpha}, h, \alpha, \beta, \gamma)$ and aerodynamic moment $M(\dot{h}, \dot{\alpha}, h, \alpha, \beta, \gamma)$ are given as

$$\begin{aligned} L &= \rho U_\infty^2 bsC_{l\alpha}\left(\alpha + \frac{\dot{h}}{U_\infty} + \left(\frac{1}{2} - a\right)b\frac{\dot{\alpha}}{U_\infty}\right) + \rho U_\infty^2 bsC_{l\beta}\beta \\ &\quad + \rho U_\infty^2 bsC_{l\gamma}\gamma \\ M &= \rho U_\infty^2 b^2 sC_{m\alpha-\text{eff}}\left(\alpha + \frac{\dot{h}}{U_\infty} + \left(\frac{1}{2} - a\right)b\frac{\dot{\alpha}}{U_\infty}\right) \\ &\quad + \rho U_\infty^2 b^2 sC_{m\beta-\text{eff}}\beta + \rho U_\infty^2 b^2 sC_{m\gamma-\text{eff}}\gamma \end{aligned} \tag{2}$$

where $C_{m\alpha-\text{eff}}$, $C_{m\beta-\text{eff}}$, and $C_{m\gamma-\text{eff}}$ are defined as follows

$$\begin{aligned} C_{m\alpha-\text{eff}} &= \left(\frac{1}{2} + a\right)C_{l\alpha} + 2C_{m\alpha} \\ C_{m\beta-\text{eff}} &= \left(\frac{1}{2} + a\right)C_{l\beta} + 2C_{m\beta} \\ C_{m\gamma-\text{eff}} &= \left(\frac{1}{2} + a\right)C_{l\gamma} + 2C_{m\gamma} \end{aligned} \tag{3}$$

The aerodynamic loads due to the bounded external disturbance can be given as [38]

$$\begin{aligned} L_g &= \rho U_\infty^2 bsC_{l\alpha}w_G(\tau)/U_\infty = \rho U_\infty bsC_{l\alpha}w_G(\tau) \\ M_g &= \left(\frac{1}{2} - a\right)bL_g \end{aligned} \tag{4}$$

where $w_G(\tau)$ denotes the disturbance velocity while τ is a dimensionless time variable defined as $\tau = U_\infty t/b$. Motivated by [40], the governing Eqs. (1) can be transformed using Eq. (2) into the following input–output representation that is amenable to model-free output feedback design

$$\ddot{\mathbf{x}} = \mathbf{h}(\mathbf{x}, \dot{\mathbf{x}}) + \mathbf{w}_{hd} + \mathbf{G}_s\mathbf{u} \tag{5}$$

where $\mathbf{x} \triangleq [h, \quad \alpha]^T \in \Re^2$ is a vector of system output, $\mathbf{u} = [u_1, \quad u_2]^T \triangleq [\beta, \quad \gamma]^T \in \Re^2$ denotes the control input vector, $\mathbf{h}(\mathbf{x}, \dot{\mathbf{x}})$ contains uncertain nonlinearities due to the existence of $k_\alpha(\alpha)$, while $\mathbf{w}_{hd}$ represents bounded unknown external disturbance terms. Here

$$\mathbf{G}_s \triangleq \begin{bmatrix} g_{11} & g_{12} \\ g_{21} & g_{22} \end{bmatrix} \in \Re^{2\times 2}$$

is a constant nonsingular gain matrix for which the constant matrix entries g_{ij} are explicitly defined as follows

$$\begin{aligned} g_{11} &= -U_\infty^2\Delta^{-1}\rho bs(I_\alpha C_{l\beta} + m_w x_\alpha b^2 C_{m\beta-\text{eff}}) \\ g_{12} &= -U_\infty^2\Delta^{-1}\rho bs(I_\alpha C_{l\gamma} + m_w x_\alpha b^2 C_{m\gamma-\text{eff}}) \\ g_{21} &= U_\infty^2\Delta^{-1}\rho bs(m_w x_\alpha bC_{l\beta} + m_T bC_{m\beta-\text{eff}}) \\ g_{22} &= U_\infty^2\Delta^{-1}\rho bs(m_w x_\alpha bC_{l\gamma} + m_T bC_{m\gamma-\text{eff}}) \end{aligned} \tag{6}$$

where $\Delta \triangleq \det(\mathbf{G}_s) = m_T I_\alpha - m_w^2 x_\alpha^2 b^2 \neq 0$. Based on the matrix decomposition introduced in [41] and the facts that both the leading principal minors g_{11} and Δ are nonzero, $\mathbf{G}_s$ can be decomposed as $\mathbf{G}_s = \mathbf{SDU}$ where $\mathbf{S}$ is a symmetric, positive-definite matrix, $\mathbf{D}$ is a diagonal matrix with diagonal entries $+1$ or -1, and $\mathbf{U}$ is an unknown unity upper triangular matrix. This $\mathbf{SDU}$ decomposition is a key factor in the proposed algebraic-loop free controller design. According to the $\mathbf{SDU}$ decomposition result previously obtained in [36], $\mathbf{S}$, $\mathbf{D}$, and $\mathbf{U}$ can be explicitly written as

$$\mathbf{S} = \begin{bmatrix} |g_{11}| & \text{sign}(g_{11})g_{21} \\ \text{sign}(g_{11})g_{21} & \text{sign}(g_{11})\text{sign}(\Delta)[g_{22} - g_{11}^{-1}g_{21}(g_{12} - g_{21}\text{sign}(\Delta))] \end{bmatrix}, \quad \mathbf{D} = \begin{bmatrix} \text{sign}(g_{11}) & 0 \\ 0 & \text{sign}(g_{11})\text{sign}(\Delta) \end{bmatrix}$$
$$\mathbf{U} = \begin{bmatrix} 1 & \frac{|g_{11}^{-1}|(g_{12} - g_{21}\text{sign}(\Delta))}{\text{sign}(g_{11})} \\ 0 & 1 \end{bmatrix} \tag{7}$$

where the notation sign $(\cdot)$ denotes the standard signum function. For purposes of control design, we assume that the signs of the leading principal minors of the high-frequency gain matrix $\mathbf{G}_s$ are known, i.e., the diagonal matrix $\mathbf{D}$ is assumed to be known. After applying the matrix decomposition property and multiplying both sides of Eq. (5) with $\mathbf{T} \triangleq \mathbf{S}^{-1} \in \Re^{2\times 2}$, Eq. (5) can be rewritten as

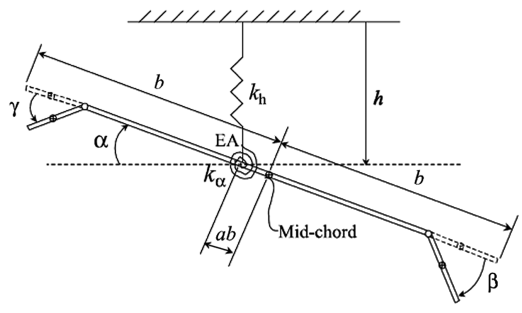

Fig. 1 Two-DOF aeroelastic system with both leading- and trailing-edge control surfaces.

$$\mathbf{T}\ddot{\mathbf{x}} = \mathbf{f}(\mathbf{x}, \dot{\mathbf{x}}) + \mathbf{w}_d + \mathbf{D}\mathbf{U}\mathbf{u} \tag{8}$$

where $\mathbf{T}$ is a symmetric, positive-definite matrix, $\mathbf{f}(\mathbf{x}, \dot{\mathbf{x}}) \triangleq \mathbf{S}^{-1}\mathbf{h}(\mathbf{x}, \dot{\mathbf{x}}) \in \Re^2$ contains unmodeled nonlinearities, while $\mathbf{w}_d \triangleq \mathbf{S}^{-1}\mathbf{w}_{hd} \in \Re^2$ represents a bounded unknown external disturbance term.

The tracking error $\mathbf{e}_1(t) \in \Re^2$ for the aeroelastic system can be defined as $\mathbf{e}_1 \triangleq \mathbf{x}_d - \mathbf{x}$. Here, $\mathbf{x}_d \in \Re^2$ is the desired output vector that is designed to be $\mathcal{C}^2$ smooth in deference to the requirements of the subsequent control design. Since the control objective is to suppress the aeroelastic vibrations, one can simply choose $\mathbf{x}_d$ to be zero all the time or use another desirable smooth trajectory $\mathbf{x}_d$ along which the actual pitching and plunging variables encoded by $\mathbf{x}$ can be driven toward the origin (by virtue of the subsequent control design). Next, to simplify the subsequent control design, the auxiliary error signals $\mathbf{e}_2(t) \in \Re^2$ and filtered tracking error $\mathbf{r}(t) \in \Re^2$ are introduced as follows

$$\mathbf{e}_2 = \dot{\mathbf{e}}_1 + \mathbf{e}_1, \qquad \mathbf{r} = \mathbf{e}_2 + \mathbf{e}_1 \tag{9}$$

Then, based on above definitions, a composite error signal can be defined as follows

$$\mathbf{z} \triangleq [\,\mathbf{e}_1^T, \quad \mathbf{e}_2^T, \quad \mathbf{r}^T\,]^T$$

By taking the time derivative of $\mathbf{r}$ and substituting from the derivative of $\mathbf{e}_2$, one can easily obtain the following relation

$$\dot{\mathbf{r}} = \ddot{\mathbf{e}}_2 + 2\dot{\mathbf{e}}_1 \tag{10}$$

After premultiplying both sides of Eq. (10) by $\mathbf{T}$ and applying the definitions given in Eqs. (8–10) can be rewritten as

$$\mathbf{T}\dot{\mathbf{r}} = \mathbf{T}(\ddot{\mathbf{x}}_d + 2\dot{\mathbf{e}}_1) - \mathbf{f}(\mathbf{x}, \dot{\mathbf{x}}) - \mathbf{w}_d - \mathbf{D}\mathbf{U}\mathbf{u} \tag{11}$$

Furthermore, given a strictly upper triangular matrix $\bar{\mathbf{U}} = \mathbf{D}\mathbf{U} - \mathbf{D}$, the open-loop dynamics of Eq. (11) can be rewritten as follows

$$\mathbf{T}\dot{\mathbf{r}} = \mathbf{T}(\ddot{\mathbf{x}}_d + 2\dot{\mathbf{e}}_1) - \mathbf{f}(\mathbf{x}, \dot{\mathbf{x}}) - \mathbf{w}_d - \bar{\mathbf{U}}\mathbf{u} - \mathbf{D}\mathbf{u} \tag{12}$$

III. State Feedback Control Development

A. Full-State Feedback Control Design

In this section, it is assumed that both the output vector $\mathbf{x}$ and their first-HYPH-order time derivative $\dot{\mathbf{x}}$ can be measured directly. As previously stated, $\mathbf{f}(\mathbf{x}, \dot{\mathbf{x}})$ denotes unmodeled system nonlinearities while $\mathbf{w}_d$ represents a bounded unknown external disturbance term. Furthermore, $\mathbf{T}$ and $\bar{\mathbf{U}}$ are assumed to be unknown while the diagonal matrix $\mathbf{D}$ comprising the signs of the leading principal minors of $\mathbf{G}_s$ is assumed to be known. Given these assumptions, the following full-state feedback control law is proposed

$$\mathbf{u} = \mathbf{D}^{-1}[\mathbf{K}\mathbf{r} + \hat{\mathbf{N}} - \mathbf{v}] \tag{13}$$

where $\mathbf{K} = \mathbf{K}_v + \mathbf{K}_d + \mathbf{K}_\lambda$ with $\mathbf{K}_v = k_v\mathbf{I}_{2\times 2}, \mathbf{K}_d = k_d\mathbf{I}_{2\times 2}, \mathbf{K}_\lambda = \text{diag}\{\,k_{\Lambda_1}, \quad 0\,\}$ while $\hat{\mathbf{N}}$ and $\mathbf{v}$ represent the feedforward compensator and robustifying term, respectively, to be designed later. After substituting Eq. (13) into the open-loop dynamics of Eq. (12) and rearranging some terms, one can obtain the following closed-loop dynamics

$$\begin{aligned}\mathbf{T}\dot{\mathbf{r}} = {} & -\mathbf{K}_d\mathbf{e}_2 + \mathbf{T}(\ddot{\mathbf{x}}_d + 2\dot{\mathbf{e}}_1) - \mathbf{f}(\mathbf{x}, \dot{\mathbf{x}}) + \mathbf{K}_d\mathbf{e}_2 - \mathbf{w}_d - \bar{\mathbf{U}}\mathbf{u} \\ & - (\mathbf{K}_v + \mathbf{K}_d + \mathbf{K}_\lambda)\mathbf{r} - \hat{\mathbf{N}} + \mathbf{v}\end{aligned} \tag{14}$$

where $\mathbf{K}_d\mathbf{e}_2$ has been added and subtracted in the above equation. In the above open-loop dynamics, $\mathbf{T}(\ddot{\mathbf{x}}_d + 2\dot{\mathbf{e}}_1)$, $\mathbf{f}(\mathbf{x}, \dot{\mathbf{x}})$, $\bar{\mathbf{U}}\mathbf{u}$, and $\mathbf{w}_d$ represent unknown system model and external disturbance as previously stated. These terms will be dealt with by using nonlinear damping and feedforward compensation. To facilitate further development, one can define the auxiliary signals Λ and Φ as follows

$$\Lambda = d_2^{-1}\bar{U}_{12}K_{22}r_2 = \rho_\Lambda r_2, \qquad \Phi = d_2^{-1}\bar{U}_{12}(\hat{N}_2 - v_2) \tag{15}$$

where d_i denotes the ith diagonal element of $\mathbf{D}^{-1}$, K_{ij} and $\bar{U}_{ij}$ represent the ijth element of the matrices $\mathbf{K}$ and $\bar{\mathbf{U}}$, respectively, while $\rho_\Lambda \triangleq d_2^{-1}\bar{U}_{12}K_{22}$ is an unknown constant scalar since $\bar{\mathbf{U}}$ is unknown. Based on the control input defined in Eq. (13) and the definitions given in Eq. (15), the vector $\bar{\mathbf{U}}\mathbf{u}$ in Eq. (12) can be written as follows

$$\bar{\mathbf{U}}\mathbf{u} = [\,\bar{U}_{12}u_2, \quad 0\,]^T = [\,\Lambda + \Phi, \quad 0\,]^T \tag{16}$$

where u_i denotes the ith element of the control input vector $\mathbf{u}$. By employing Eq. (16) and rearranging some terms, the closed-loop dynamics of Eq. (14) can be rewritten as follows

$$\begin{aligned}\mathbf{T}\dot{\mathbf{r}} = {} & -\mathbf{K}_d\mathbf{e}_2 - (\mathbf{K}_d + \mathbf{K}_\lambda)\mathbf{r} - [\,\Lambda, \quad 0\,]^T - \mathbf{K}_v\mathbf{r} + \mathbf{T}(\ddot{\mathbf{x}}_d + 2\dot{\mathbf{e}}_1) \\ & - \mathbf{f}(\mathbf{x}, \dot{\mathbf{x}}) + \mathbf{K}_d\mathbf{e}_2 - [\,\Phi, \quad 0\,]^T - \hat{\mathbf{N}} - \mathbf{w}_d + \mathbf{v}\end{aligned} \tag{17}$$

Given the expression of Eq. (17), a nonlinear target function $\mathbf{N} \in \Re^2$, which contains the unknown system vectors $\mathbf{T}(\cdot)$ and $\mathbf{f}(\cdot)$, can be defined as follows

$$\mathbf{N}(\bar{\mathbf{x}}_t) = \mathbf{T}(\ddot{\mathbf{x}}_d + 2\dot{\mathbf{e}}_1) - \mathbf{f}(\mathbf{x}, \dot{\mathbf{x}}) + \mathbf{K}_d\mathbf{e}_2 - [\,\Phi, \quad 0\,]^T \tag{18}$$

Here, the input vector $\bar{\mathbf{x}}_t \in \Re^{11}$ for the nonlinear target function can be defined as follows

$$\bar{\mathbf{x}}_t = [\,\mathbf{x}^T, \quad \dot{\mathbf{x}}^T, \quad \mathbf{x}_d^T, \quad \dot{\mathbf{x}}_d^T, \quad \ddot{\mathbf{x}}_d^T, \quad \|\hat{\mathbf{Z}}\|_F\,]^T \tag{19}$$

where $\|\cdot\|_F$ denotes the Frobenius norm and $\hat{\mathbf{Z}}$ is a composite weight matrix estimate which will be subsequently designed. In a later section, a feedforward compensator $\hat{\mathbf{N}}$ will be designed to compensate this nonlinear target function $\mathbf{N}$ which contains the unknown system model. To facilitate the stability analysis in the following section, $\mathbf{\Pi}$ and $\mathbf{\Psi}$ can be defined by using the definitions in Eqs. (15) and (18) as follows

$$\mathbf{\Pi} = -[\,\Lambda, \quad 0\,]^T, \qquad \mathbf{\Psi} = -\mathbf{K}_v\mathbf{r} + \mathbf{N} - \hat{\mathbf{N}} - \mathbf{w}_d + \mathbf{v} \tag{20}$$

After employing Eqs. (18) and (20), one can finally rewrite the closed-loop dynamics of Eq. (17) as

$$\mathbf{T}\dot{\mathbf{r}} = -\mathbf{K}_d\mathbf{e}_2 - (\mathbf{K}_d + \mathbf{K}_\lambda)\mathbf{r} + \mathbf{\Pi} + \mathbf{\Psi} \tag{21}$$

It will be subsequently shown how the unknown term $\mathbf{\Pi}$ can be nonlinearly damped out by the feedback control term $(\mathbf{K}_d + \mathbf{K}_\lambda)\mathbf{r}$ and how the feedforward compensator $\hat{\mathbf{N}}$ and robustifying term $\mathbf{v}$ can be designed to compensate for the unknown terms $\mathbf{T}(\ddot{\mathbf{x}}_d + 2\dot{\mathbf{e}}_1)$, $\mathbf{f}(\mathbf{x}, \dot{\mathbf{x}})$, and $[\,\Phi, \quad 0\,]^T$.

B. Feedforward Compensator Design

Since the model of the wing section and external disturbance are assumed to be unknown in the control design, adaptive control designs cannot be applied. In lieu of adaptation, a neural network feedforward compensator $\hat{\mathbf{N}}$ along with robustifying term $\mathbf{v}$ are proposed to compensate for this target function $\mathbf{N}$ and the disturbance signal $\mathbf{w}_d$; thus, model-free control design is facilitated by exploiting the twin neural properties of universal approximation and online (i.e., real-time) learning.

The nonlinear target function $\mathbf{N}$ defined in Eq. (18) can be approximated as a three-layer neural network target function of the form [42]

$$\mathbf{N}(\bar{\mathbf{x}}) = \mathbf{W}^T\boldsymbol{\sigma}(\mathbf{V}^T\bar{\mathbf{x}}) + \boldsymbol{\epsilon}(\bar{\mathbf{x}}) \tag{22}$$

where $\bar{\mathbf{x}} = [\,1, \quad \bar{\mathbf{x}}_t^T\,]^T \in \Re^{p_1+1}$ denotes the augmented input vector while $\boldsymbol{\sigma}(\cdot) \in \Re^{p_2+1}$ denotes the activation function; in this paper, a sigmoid function is chosen as the activation function. $\boldsymbol{\epsilon}(\bar{\mathbf{x}}) \in \Re^{p_3}$ is the functional reconstruction error vector, $\mathbf{V} \in \Re^{(p_1+1)\times p_2}$ is the ideal first layer interconnection weight matrix between input layer and hidden layer, $\mathbf{W} \in \Re^{(p_2+1)\times p_3}$ denotes the ideal second layer interconnection weight matrix between hidden layer and output layer, while $p_1 + 1$, $p_2 + 1$, and p_3 are the number of nodes in the input layer, hidden layer, and output layer, respectively. Note that the input vector $\bar{\mathbf{x}}$ and $\boldsymbol{\sigma}(\cdot)$ are augmented vectors because of placement of 1 as their first element since thresholds are included as the first columns of the weight matrices $\mathbf{W}$ and $\mathbf{V}$. For the problem at hand, it will be assumed that the ideal weight matrices $\mathbf{W}$ and $\mathbf{V}$ are constant and bounded such that $\|\mathbf{W}\|_F \leq \mathbf{W}_B$ and $\|\mathbf{V}\|_F \leq \mathbf{V}_B$, where $\mathbf{W}_B$ and $\mathbf{V}_B$ are positive constants and $\|\cdot\|_F$ denotes the Frobenius norm. The approximation error is assumed to be bounded in a compact set by $\|\boldsymbol{\epsilon}(\bar{\mathbf{x}})\| < \epsilon_N$ where ϵ_N is an unknown positive constant related to the number of nodes in the hidden layer. Based on Eq. (22), the typical three-level neural network compensator for target function $\mathbf{N}(\bar{\mathbf{x}})$ is given in the following form

$$\hat{\mathbf{N}}(\bar{\mathbf{x}}) = \hat{\mathbf{W}}^T \boldsymbol{\sigma}(\hat{\mathbf{V}}^T \bar{\mathbf{x}}) \tag{23}$$

where $\hat{\mathbf{W}}$ and $\hat{\mathbf{V}}$ are estimated weight matrices. In this paper, $\hat{\mathbf{W}}$ and $\hat{\mathbf{V}}$ can be set to zero at first or randomly initialized within certain region, which implies that there is no requirement for preliminary offline learning phase for the neural network. Motivated by [42] and the ensuing stability analysis, the estimated weight matrices can be updated or learned through online weight tuning algorithms of the form

$$\begin{aligned} \dot{\hat{\mathbf{W}}} &= (\mathbf{F}\hat{\boldsymbol{\sigma}} - \mathbf{F}\hat{\boldsymbol{\sigma}}'\hat{\mathbf{V}}^T\bar{\mathbf{x}})\mathbf{r}^T - \kappa\mathbf{F}\|\mathbf{r}\|\hat{\mathbf{W}} \\ \dot{\hat{\mathbf{V}}} &= \mathbf{G}\bar{\mathbf{x}}(\hat{\boldsymbol{\sigma}}'^T\hat{\mathbf{W}}\mathbf{r}^T)^T - \kappa\mathbf{G}\|\mathbf{r}\|\hat{\mathbf{V}} \end{aligned} \tag{24}$$

where $\mathbf{F} \in \Re^{(p_2+1)\times(p_2+1)}$ and $\mathbf{G} \in \Re^{(p_1+1)\times(p_1+1)}$ are positive-definite, diagonal gain matrices, $\kappa > 0$ is a scalar design parameter, $\hat{\boldsymbol{\sigma}} = \boldsymbol{\sigma}(\hat{\mathbf{V}}^T\bar{\mathbf{x}})$ and $\hat{\boldsymbol{\sigma}}' \equiv d\boldsymbol{\sigma}(\hat{\mathbf{V}}^T\bar{\mathbf{x}})/d(\hat{\mathbf{V}}^T\bar{\mathbf{x}})$. After substituting Eqs. (22) and (23) into Eq. (20) and applying a Taylor series expansion, $\boldsymbol{\Psi}$ defined in Eq. (20) can be given as

$$\boldsymbol{\Psi} = -\mathbf{K}_v\mathbf{r} + \tilde{\mathbf{W}}^T[\hat{\boldsymbol{\sigma}} - \hat{\boldsymbol{\sigma}}'\hat{\mathbf{V}}^T\bar{\mathbf{x}}] + \hat{\mathbf{W}}^T\hat{\boldsymbol{\sigma}}'\tilde{\mathbf{V}}^T\bar{\mathbf{x}} + \mathbf{w} + v \tag{25}$$

where $\tilde{\mathbf{W}} = \mathbf{W} - \hat{\mathbf{W}}$ and $\tilde{\mathbf{V}} = \mathbf{V} - \hat{\mathbf{V}}$ denote weight matrices estimation errors while $\mathbf{w}$ can be written as

$$\mathbf{w} = \tilde{\mathbf{W}}^T\hat{\boldsymbol{\sigma}}'\mathbf{V}^T\bar{\mathbf{x}} + \tilde{\mathbf{W}}^T O(\tilde{\mathbf{V}}^T\bar{\mathbf{x}})^2 + \epsilon(\bar{\mathbf{x}}) - \mathbf{w}_d \tag{26}$$

To facilitate the subsequent analysis, one can also obtain a compact form representation for $\|\mathbf{w}\|$ as follows

$$\|\mathbf{w}\| = C_0 + C_1\|\tilde{\mathbf{Z}}\|_F + C_2\|\tilde{\mathbf{Z}}\|_F\|\mathbf{r}\| \tag{27}$$

where C_0, C_1, and C_2 are all positive constants while the ideal composite weight matrix $\mathbf{Z}$, estimated composite weight matrix $\hat{\mathbf{Z}}$, and the composite weight mismatch matrix $\tilde{\mathbf{Z}}$ are defined as follows

$$\mathbf{Z} = \begin{bmatrix} \mathbf{W} & \mathbf{0} \\ \mathbf{0} & \mathbf{V} \end{bmatrix}, \qquad \hat{\mathbf{Z}} \equiv \begin{bmatrix} \hat{\mathbf{W}} & \mathbf{0} \\ \mathbf{0} & \hat{\mathbf{V}} \end{bmatrix}, \qquad \tilde{\mathbf{Z}} \equiv \begin{bmatrix} \tilde{\mathbf{W}} & \mathbf{0} \\ \mathbf{0} & \tilde{\mathbf{V}} \end{bmatrix} \tag{28}$$

where $\tilde{\mathbf{Z}} = \mathbf{Z} - \hat{\mathbf{Z}}$. According to the boundedness property for $\|\mathbf{W}\|_F$ and $\|\mathbf{V}\|_F$, it is assumed that there exists a constant Z_B such that $Z_B > \|\mathbf{Z}\|_F$. Based on the definition of Z_B, the robustifying term $\mathbf{v}$ in Eq. (13) can be defined as

$$\mathbf{v} = -K_z(\|\hat{\mathbf{Z}}\|_F + Z_B)\mathbf{r} \tag{29}$$

where K_z is a positive constant. Finally, it is noted that the unknown external disturbance $\mathbf{w}_d$ and functional reconstruction error $\epsilon(\bar{\mathbf{x}})$ are assumed to be bounded.

C. Stability Analysis

The stability analysis for the proposed model-free controller is provided in the following theorem. To facilitate ease of expression, the stability analysis is split into two parts which comprise components of the derivative of the Lyapunov function. While the first part shows the usefulness of the nonlinear damping technique, the second part shows the utility of the feedforward compensator and the robustifying injection term in proving system stability. A uniformly ultimately bounded (UUB) result is obtained for both the norm of the filtered tracking error $\mathbf{r}$ and the norm of the neural network weight estimation error $\tilde{\mathbf{Z}}$. Note a signal is uniformly ultimately bounded [43] if there exist positive constants b and c, independent of $t_0 \geq 0$, and for every $a \in (0, c)$, there is $T = T(a, b) \geq 0$, independent of t_0, such that

$$\|x(t_0)\| \leq a \Rightarrow \|x(t)\| \leq b, \quad \forall\ t \geq t_0 + T$$

Theorem 1: Provided the control gain matrix $\mathbf{K}$ defined in Eq. (13) is chosen to be appropriately large, the error signals ($\mathbf{r}$ and $\tilde{\mathbf{Z}}$) for the closed-loop system defined in Eq. (21) are UUB.

Proof: First, a nonnegative Lyapunov function candidate V_0 is defined as

$$V_0 = \frac{1}{2}\mathbf{e}_1^T\mathbf{K}_d\mathbf{e}_1 + \frac{1}{2}\mathbf{r}^T\mathbf{T}\mathbf{r} + \frac{1}{2}\mathrm{tr}\{\tilde{\mathbf{W}}^T\mathbf{F}^{-1}\tilde{\mathbf{W}}\} + \frac{1}{2}\mathrm{tr}\{\tilde{\mathbf{V}}^T\mathbf{G}^{-1}\tilde{\mathbf{V}}\} \tag{30}$$

After differentiating Eq. (30) and using the results obtained in Eqs. (21) and (25), the following expressions are obtained

$$\dot{V}_0 = \dot{V}_1 + \dot{V}_2 \tag{31}$$

where

$$\begin{aligned} \dot{V}_1 &= \mathbf{e}_1^T\mathbf{K}_d\dot{\mathbf{e}}_1 - \mathbf{r}^T\mathbf{K}_d\mathbf{e}_2 + \mathbf{r}^T[-(\mathbf{K}_d + \mathbf{K}_\lambda)\mathbf{r} + \boldsymbol{\Pi}] \\ \dot{V}_2 &= \mathbf{r}^T\boldsymbol{\Psi} + \mathrm{tr}\{\tilde{\mathbf{W}}^T\mathbf{F}^{-1}\dot{\tilde{\mathbf{W}}}\} + \mathrm{tr}\{\tilde{\mathbf{V}}^T\mathbf{G}^{-1}\dot{\tilde{\mathbf{V}}}\} \end{aligned} \tag{32}$$

After using the error definitions of Eq. (9), one can obtain the following expression for $\dot{V}_1$

$$\dot{V}_1 = -\mathbf{e}_1^T\mathbf{K}_d\mathbf{e}_1 - \mathbf{e}_2^T\mathbf{K}_d\mathbf{e}_2 - \mathbf{r}^T\mathbf{K}_d\mathbf{r} - \mathbf{r}^T\mathbf{K}_\lambda\mathbf{r} + \mathbf{r}^T\boldsymbol{\Pi} \tag{33}$$

which can be upperbounded by employing the definitions of $\mathbf{z}$, $\boldsymbol{\Pi}$, Λ, k_{Λ_1}, and k_d as follows

$$\dot{V}_1 \leq -k_d\|\mathbf{z}\|^2 + [\|\rho_\Lambda\|\|\mathbf{z}\|\|\mathbf{r}_1\| - k_{\Lambda_1}\|\mathbf{r}_1\|^2] \tag{34}$$

where Eq. (15) has been used to obtain the fact that $\|\Lambda\| < \|\rho_\Lambda\|\|\mathbf{z}\|$. After completing the squares on the bracketed term in Eq. (34), the following upperbound is obtained

$$\dot{V}_1 \leq -\left(k_d - \frac{\|\rho_\Lambda\|^2}{4k_{\Lambda_1}}\right)\|\mathbf{z}\|^2 \tag{35}$$

By choosing k_d and k_{Λ_1} large enough such that bracketed term in Eq. (35) is positive, one can easily see that $\dot{V}_1$ in Eq. (35) can be upperbounded as follows

$$\dot{V}_1 \leq -\gamma(\|\mathbf{z}\|^2) \tag{36}$$

where $\gamma(\|\mathbf{z}\|^2)$ is a class $\mathcal{K}_\infty$ function. Next, by substituting the expression for $\boldsymbol{\Psi}$ given in (25), $\dot{V}_2$ can be obtained as follows

$$\begin{aligned} \dot{V}_2 = {} & \mathbf{r}^T[-\mathbf{K}_v\mathbf{r} + \tilde{\mathbf{W}}^T[\hat{\boldsymbol{\sigma}} - \hat{\boldsymbol{\sigma}}'\hat{\mathbf{V}}^T\bar{\mathbf{x}}] + \hat{\mathbf{W}}^T\hat{\boldsymbol{\sigma}}'\tilde{\mathbf{V}}^T\bar{\mathbf{x}} + \mathbf{w} + \mathbf{v}] \\ & + \mathrm{tr}\{\tilde{\mathbf{W}}^T\mathbf{F}^{-1}\dot{\tilde{\mathbf{W}}}\} + \mathrm{tr}\{\tilde{\mathbf{V}}^T\mathbf{G}^{-1}\dot{\tilde{\mathbf{V}}}\} \end{aligned} \tag{37}$$

After applying the update laws designed in Eq. (24), canceling out the matched terms, and using the definitions of Eqs. (28) and (37) can be upperbounded as follows

$$\dot{V}_2 \leq -\mathbf{r}^T\mathbf{K}_v\mathbf{r} + \kappa\|\mathbf{r}\|\mathrm{tr}\{\tilde{\mathbf{Z}}^T(\mathbf{Z} - \tilde{\mathbf{Z}})\} + \|\mathbf{r}\|\|\mathbf{w}\| + \mathbf{r}^T\mathbf{v} \tag{38}$$

By substituting Eqs. (27) and (29) into Eq. (38), it is possible to further upperbound $\dot{V}_2$ as

$$\dot{V}_2 \leq -\|\mathbf{r}\|[\mathbf{K}_{v_{\min}}\|\mathbf{r}\| - \kappa\|\tilde{\mathbf{Z}}\|_F(Z_B - \|\tilde{\mathbf{Z}}\|_F) - C_0 - C_1\|\tilde{\mathbf{Z}}\|_F - C_2\|\tilde{\mathbf{Z}}\|_F\|\mathbf{r}\| + K_z(\|\hat{\mathbf{Z}}\|_F + Z_B)\|\mathbf{r}\|] \quad (39)$$

where the following relation has been used to derive (39)

$$\mathrm{tr}\{\tilde{\mathbf{Z}}^T(\mathbf{Z} - \tilde{\mathbf{Z}})\} = \langle \tilde{\mathbf{Z}}, \quad \mathbf{Z} \rangle - \|\tilde{\mathbf{Z}}\|_F^2 \leq \|\tilde{\mathbf{Z}}\|_F\|\mathbf{Z}\|_F - \|\tilde{\mathbf{Z}}\|_F^2 \leq \|\tilde{\mathbf{Z}}\|_F Z_B - \|\tilde{\mathbf{Z}}\|_F^2 \quad (40)$$

Based on the fact that $\|\hat{\mathbf{Z}}\|_F + Z_B > \|\tilde{\mathbf{Z}}\|_F$, one can choose $K_z > C_2$ such that Eq. (39) can be rewritten as

$$\dot{V}_2 \leq -\|\mathbf{r}\|[\mathbf{K}_{v_{\min}}\|\mathbf{r}\| - \kappa\|\tilde{\mathbf{Z}}\|_F(Z_B - \|\tilde{\mathbf{Z}}\|_F) - C_0 - C_1\|\tilde{\mathbf{Z}}\|_F] \quad (41)$$

By defining $C_3 = Z_B + C_1/\kappa$, Eq. (41) can be rewritten as follows

$$\dot{V}_2 \leq -\|\mathbf{r}\|[K_{v_{\min}}\|\mathbf{r}\| + \kappa(\|\tilde{\mathbf{Z}}\|_F - C_3/2)^2 - C_0 - \kappa C_3^2/4] \quad (42)$$

where $K_{v_{\min}}$ denotes the minimum singular value of $\mathbf{K}_v$. Combining with Eqs. (36) and (31) can be upperbounded as follows

$$\dot{V}_0 \leq -\gamma(\|\mathbf{z}\|^2) - \|\mathbf{r}\|[K_{v_{\min}}\|\mathbf{r}\| + \kappa(\|\tilde{\mathbf{Z}}\|_F - C_3/2)^2 - C_0 - \kappa C_3^2/4] \quad (43)$$

It is straightforward to see that Eq. (43) is guaranteed negative as long as either

$$\|\mathbf{r}\| > \frac{C_0 + \kappa C_3^2/4}{K_{v_{\min}}} \equiv b_r \quad \text{or} \quad \|\tilde{\mathbf{Z}}\|_F > C_3/2 + \sqrt{C_0 + \kappa C_3^2/4} \equiv b_Z \quad (44)$$

Thus, $\dot{V}_0$ is negative outside the compact set $\{\|\mathbf{r}\| \leq b_r, \|\tilde{\mathbf{Z}}\|_F \leq b_Z\}$. Now, LaSalle extension in [44] can be used to prove the UUB results for both $\|\mathbf{r}\|$ and $\|\tilde{\mathbf{Z}}\|_F$. It is easy to see from Eq. (44) that the size of the ultimate bound b_r for $\|\mathbf{r}\|$ can be made smaller by increasing the size of the control gain. We note here that the gain matrix $\mathbf{K}$ needs to be chosen *appropriately large* in the sense that the selections for k_d and k_{Λ_1} are made to ensure that the parenthesized term in Eq. (35) is positive. □

IV. Output Feedback Control Development

In this section, we assume that the only measurements available are the pitching and plunging displacements; thus, the remaining states are estimated through the use of a HGO. When $\mathbf{x}(t)$ is the output of the system and the only measurable state vector, the sole measurable error signal is $\mathbf{e}_1(t)$, given the knowledge of $\mathbf{x}(t)$ and $\mathbf{x}_d(t)$. Motivated by the result in [45], an estimate $\hat{\mathbf{z}}(t) = [\hat{\mathbf{e}}_1^T, \quad \hat{\mathbf{e}}_2^T, \quad \hat{\mathbf{r}}^T]^T \in \Re^6$ for the auxiliary error signal $\mathbf{z}(t)$ can be obtained via the following HGO

$$\dot{\hat{\mathbf{e}}}_1 = \hat{\mathbf{r}} - 2\hat{\mathbf{e}}_1 + \frac{\alpha_1}{\bar{\epsilon}}(\mathbf{e}_1 - \hat{\mathbf{e}}_1) \quad \text{and} \quad \dot{\hat{\mathbf{r}}} = \frac{\alpha_2}{\bar{\epsilon}^2}(\mathbf{e}_1 - \hat{\mathbf{e}}_1) \quad (45)$$

where $\alpha_i \in \Re^{m\times m} \ \forall \ i = 1, 2$ are gain constants and $\bar{\epsilon}$ is a small positive constant. Note that $\hat{\mathbf{e}}_2 = \hat{\mathbf{r}} - \hat{\mathbf{e}}_1$. To suppress the peaking phenomenon due to using HGO, we modify the full-state control design of Eq. (13) to an output feedback saturated control as follows

$$\mathbf{u} = \mathrm{sat}[\mathbf{D}^{-1}(\mathbf{K}\hat{\mathbf{r}} + \hat{\mathbf{N}} - \mathbf{v})] \quad (46)$$

where $\mathrm{sat}(\cdot)$ denotes the standard saturation function and saturation is applied outside an appropriately defined compact set for the control input $\mathbf{u}$. Here, $\hat{\mathbf{N}}$ and $\mathbf{v}$ have been defined in the same manner as in Eq. (13). For details of the stability analysis of the output feedback control design, the reader is referred to [45].

As we can see in Eq. (46), the proposed OFB controller only depends on the estimated filtered tracking error $\hat{\mathbf{r}}$, known diagonal matrix $\mathbf{D}$, feedforward compensator $\hat{\mathbf{N}}$, and the robustifying term $\mathbf{v}$. The update laws for the weight matrices of the feedforward compensator $\hat{\mathbf{N}}$ and robustifying term $\mathbf{v}$ are determined by the estimated filtered tracking error $\hat{\mathbf{r}}$ while all the other constants and control gains can be chosen to satisfy appropriate performance metrics. The aforementioned facts imply that this OFB control law uses very little information about system structure and parameters compared with the adaptive controller designed in [36]. Specifically, the only knowledge about the model we need is the signs of the leading principal minors of the input gain matrix $\mathbf{G}_s$.

Remark 1: Based on observer theory, it is well known that there is a trade off between the speed of state reconstruction and the immunity to measurement noise [46]. Although the high-gain observer could quickly reconstruct the system unknown states by using a large enough observer gain, large gain would undesirably magnify the measurement noise [47]. A switched gain strategy can be found in [46] to address this problem.

V. Simulations and Results

A. Wing Section and Disturbance Model

In this section, simulation results were presented for a nonlinear 2-DOF aeroelastic system controlled by leading- and trailing-edge flaps and subjected to external disturbances. The nonlinear wing section model was simulated using the dynamics of Eqs. (1) and (2). The model parameters used in the simulation were the same as used in [33] and listed in Table 1. In particular, the pitching spring stiffness $k_\alpha(\alpha)$ was modeled as a polynomial nonlinearity as shown in Table 1. Note that all these parameters were used to simulate the wing model but were considered unknown for the purpose of control design.

Similar to [33,36], the desired trajectory variables $\mathbf{x}_d$, $\dot{\mathbf{x}}_d$, and $\ddot{\mathbf{x}}_d$ were simply selected as zero. The initial conditions for pitch angle $\alpha(t)$ and plunge displacement $h(t)$ were chosen as $\alpha(0) = 5.729$ [deg] and $h(0) = 0$ [m] while all other variables $\dot{h}(t)$, $\dot{\alpha}(t)$, $\ddot{h}(t)$, and $\ddot{\alpha}(t)$ were initially set to zero. Both the leading-edge $\beta(t)$ and trailing-edge $\gamma(t)$ flaps were constrained to vary between ± 15 [deg]. For the numerical example, the signs of the leading principal minors of the high-frequency gain matrix $\mathbf{G}_s$ are encoded in the diagonal matrix $\mathbf{D}$ which can be explicitly given as

$$\mathbf{D} = \begin{bmatrix} -1 & 0 \\ 0 & -1 \end{bmatrix} \quad (47)$$

We remark that the model-free controller designed here depends only on the knowledge of $\mathbf{D}$ but not on the knowledge of $\mathbf{S}$ and $\mathbf{U}$.

Before introducing the external disturbance tested in this paper, a simple static exploration of the wing section model reveals the relation between magnitude of sustained external disturbance and the amplitude-limited control signals. First, we assume that wing section model is able to reach the desired equilibrium point (e.g., $h, \alpha, \dot{h}, \dot{\alpha}, \ddot{h}$, and $\ddot{\alpha}$ are all equal to zero) under certain types of external

Table 1 Wing section parameters

Parameter value	Parameter value
$a = -0.6719$	$b = 0.1905$, m
$s = 0.5945$, m	$\rho = 1.225$ [kg · m^3]
$r_{cg} = -b(.0998 + a)$, m	$x_a = r_{cg}/b$
$c_h = 27.43$ [kg/s]	$c_\alpha = 0.0360$ [N · s]
$k_h = 2844$ [N/m]	$m_{\text{wing}} = 4.340$, kg
$m_w = 5.23$, kg	$m_T = 15.57$, kg
$I_{cgw} = 0.04342$ [kg · m^2]	$I_{cam} = 0.04697$ [kg · m^2]
$C_{l\alpha} = 6.757$ [rad^{-1}]	$C_{m\alpha} = 0$ [rad^{-1}]
$C_{l\beta} = 3.774$ [rad^{-1}]	$C_{m\beta} = -0.6719$ [rad^{-1}]
$C_{l\gamma} = -0.1566$ [rad^{-1}]	$C_{m\gamma} = -0.1005$ [rad^{-1}]
$k_\alpha(\alpha) = 12.77 + 53.47\alpha + 1003\alpha^2$ [N · m]	
$I_\alpha = I_{cam} + I_{cgw} + m_{\text{wing}} r_{cg}^2$ [kg · m^2]	

disturbances. In this case, the left-hand side of Eq. (1) is zero, and all terms associated with $h, \alpha, \dot{h}$, and $\dot{\alpha}$ on the right-hand side of Eq. (1) are also zero. Thus, it is straightforward to see that

$$\begin{cases} \rho U_\infty^2 bsC_{l\beta}\beta + \rho U_\infty^2 bsC_{l\gamma}\gamma + \rho U_\infty bsC_{l\alpha} w_G(\tau) = 0, \\ \rho U_\infty^2 b^2 sC_{m\beta-\text{eff}}\beta + \rho U_\infty^2 b^2 sC_{m\gamma-\text{eff}}\gamma + \left(\frac{1}{2} - a\right) bL_g = 0 \end{cases} \tag{48}$$

Based on the result in Eqs. (4) and (48) can be simplified as

$$\begin{bmatrix} C_{l\beta} & C_{l\gamma} \\ C_{m\beta-\text{eff}} & C_{m\gamma-\text{eff}} \end{bmatrix} \begin{bmatrix} \beta \\ \gamma \end{bmatrix} = \begin{bmatrix} -C_{l\alpha} w_G(\tau)/U_\infty \\ -\left(\frac{1}{2} - a\right) C_{l\alpha} w_G(\tau)/U_\infty \end{bmatrix} \tag{49}$$

Assuming the 2×2 matrix in above equation is nonsingular, we have

$$\begin{bmatrix} \beta \\ \gamma \end{bmatrix} = -\frac{w_G(\tau)}{U_\infty} \begin{bmatrix} C_{l\beta} & C_{l\gamma} \\ C_{m\beta-\text{eff}} & C_{m\gamma-\text{eff}} \end{bmatrix}^{-1} \begin{bmatrix} C_{l\alpha} \\ \left(\frac{1}{2} - a\right) C_{l\alpha} \end{bmatrix} \tag{50}$$

Now, it is easy to see that given bounded control signals β and γ, one can obtain an upper bound for the magnitude of $w_G(\tau)$ depending on the flow speed U_∞. If $w_G(\tau)$ is too large with respect to the constrained control signals, Eq. (48) will not hold and the wing section model variables α and h are unable to reach the origin regardless of the type of control design. Given the parameters listed in Table 1, the maximum magnitude of the external signals cannot be larger than 0.047 [m/s] and 0.077 [m/s], corresponding to 0.58% of the velocities selected, for the two values of velocities selected in simulations, $U_\infty = 8$ [m/s] and $U_\infty = 13.28$ [m/s], respectively, to drive the plunge and pitch displacement to zero. As will be seen in the results, larger disturbance size results in alternate equilibria away from the origin.

In this paper, three kinds of external disturbances are considered according to [38]. The first type of external disturbance is modeled as a triangular gust, whose velocity distribution $w_G(\tau)$ can be given as

$$\begin{aligned} w_G(\tau) = {} & 2w_0 \frac{\tau}{\tau_G} \left(H(\tau) - H\left(\tau - \frac{\tau_G}{2}\right) \right) \\ & - 2w_0 \left(\frac{\tau}{\tau_G} - 1 \right) \left(H(\tau - \tau_G) - H\left(\tau - \frac{\tau_G}{2}\right) \right) \end{aligned} \tag{51}$$

where $H(\cdot)$ denotes a unit step function, $\tau_G = U_\infty t_G / b$ and $t_G = 0.25$ [s], and $w_0 = 0.7$ [m/s]. This triangular gust lasts 0.5 s from $t = 0$ [s] to $t = 0.5$ [s]. The second type of external disturbance, one that is sustained beyond the transient response time of the closed-loop aeroelastic system, is given in the form of graded gust, whose velocity distribution $w_G(\tau)$ can be expressed as follows

$$w_G(\tau) = H(\tau) w_0 (1 - e^{-0.75\tau}) \tag{52}$$

where w_0 is chosen according to the simulation setting. The third disturbance is given in the form of sinusoidal gust with the following velocity distribution function $w_G(\tau)$

$$w_G(\tau) = H(\tau) w_0 \sin \omega\tau \tag{53}$$

where $\omega = 0.5$ [rad/s] while w_0 is selected based on different simulation settings. Thus, these three disturbances profiles test the system response to ephemeral disturbance, steady sustained disturbance, and time-varying sustained disturbance. Also note that the triangular gust tested in our paper is very similar to the traditional 1-cosine gust-type function, both of which can be classified as ephemeral disturbances. Furthermore, a more challenging continuous sinusoidal disturbance is also tested in the following simulation.

B. Antiwindup Mechanism

In this paper, both the leading-edge $\beta(t)$ and trailing-edge $\gamma(t)$ flaps are constrained to vary between ± 15 [deg], assuming that saturation will occur outside these limits. Since the control design contains a learning component that involves integration of the error system (see Eq. (24) where $\hat{\mathbf{W}}$ and $\hat{\mathbf{V}}$ rely upon integration of the filtered error signal $\hat{\mathbf{r}}$), control input saturation is known to lead to windup problem. Motivated by back-calculation algorithm introduced in [48], we propose the following method to limit the error signal $\hat{\mathbf{r}}$ according to the magnitude of original control input $\mathbf{u}_i$ in Eq. (24) as

$$r_{b,i} = \begin{cases} g_i \hat{r}_i \dfrac{u_b}{|u_i|}, & |u_i| > u_b, \quad \forall\ i = 1, 2 \\ \hat{r}_i, & |u_i| \le u_b, \quad \forall\ i = 1, 2 \end{cases} \tag{54}$$

where $\mathbf{r}_b$ denotes the limited filtered error which is used in the neural network weight matrices update law, $\mathbf{u}$ designed in Eq. (46) denotes the actual control signal for the actuator with saturation bound $u_b = 15$ [deg], while g_i, $i = 1, 2$ denote a set of auxiliary saturation gains. After limiting the error signal $\hat{\mathbf{r}}$ according to Eq. (54), the weight matrices update law for the neural networks compensator and robustifying term are modified as follows

$$\begin{aligned} \dot{\hat{\mathbf{W}}} &= (\mathbf{F}\hat{\sigma} - \mathbf{F}\hat{\sigma}'\hat{\mathbf{V}}^T\bar{\mathbf{x}})\mathbf{r}_b^T - \kappa\mathbf{F}\|\mathbf{r}_b\|\hat{\mathbf{W}} \\ \dot{\hat{\mathbf{V}}} &= \mathbf{G}\mathbf{x}(\hat{\sigma}'^T\hat{\mathbf{W}}\mathbf{r}_b^T)^T - \kappa\mathbf{G}\|\mathbf{r}_b\|\hat{\mathbf{V}}, \qquad \mathbf{v} = -K_z(\|\hat{\mathbf{Z}}\|_F + Z_B)\mathbf{r}_b \end{aligned} \tag{55}$$

C. Controller and Observer Implementation

The output feedback control is implemented via the HGO defined in Eq. (45) and control law in Eq. (46). The parameters for the controller and observer in these simulations are listed in Table 2.

Also note that an explicit expression for $\mathbf{D}$ has been given in Eq. (47). According to the definition of $\bar{\mathbf{x}}_t$ given in Eq. (19), a choice of $p_1 = 11$ needs to be made in general. For the numerical example, however, since $\mathbf{x}_d$, $\dot{\mathbf{x}}_d$, and $\ddot{\mathbf{x}}_d$ were all bounded signals and chosen to be zero for all time, they can be removed from the input set $\bar{\mathbf{x}}_t$ to simplify the computational complexity. The simplified input set for the numerical example is $\bar{\mathbf{x}}_t = [\mathbf{x}^T, \ \dot{\mathbf{x}}^T, \ \|\hat{\mathbf{Z}}\|_F]^T \in \Re^5$ based upon which $\bar{\mathbf{x}} = [1, \ \bar{\mathbf{x}}_t]^T \in \Re^6$. Then, in the feedforward compensator used in the following simulation, p_1, p_2, and p_3 are given as $p_1 = 5$, $p_2 = 10$, $p_3 = 2$. The above selection of p_1, p_2, and p_3 implies that $\hat{\mathbf{W}} \in \Re^{11\times 2}$ and $\hat{\mathbf{V}} \in \Re^{6\times 10}$. The number of hidden layer nodes is chosen through a trial and error method to obtain best performance. A choice of $p_2 = 10$ is used since the controller performance is seen to be satisfactory for this choice. Although the approximation error is expected to reduce when the number of hidden layer nodes increases, one still needs to consider the computational efficiency, especially considering the constraints of real-time control implementation. It is well known that arbitrary choices for the initial weight matrices $\hat{\mathbf{W}}$ and $\hat{\mathbf{V}}$ may result in unacceptable transient response. By performing extensive simulations, in this paper, the initial weight matrix $\hat{\mathbf{W}}$ is chosen to be zero while the initial weights for elements of $\hat{\mathbf{V}}$ are randomly chosen between -1 and 1. Simulation results show that such a selection guarantees an acceptable transient response. The weight update laws for the neural

Table 2 Simulation parameters

Parameter	Triangular		Graded	Sinusoidal
U_∞	8 [m/s]	13.28 [m/s]	13.28 [m/s]	13.28 [m/s]
$\mathbf{K}$	$3\mathbf{I}_{2\times2}$	$0.5\mathbf{I}_{2\times2}$	$0.5\mathbf{I}_{2\times2}$	$0.5\mathbf{I}_{2\times2}$
$\mathbf{F}$	$10\mathbf{I}_{11\times11}$	$5\mathbf{I}_{11\times11}$	$5\mathbf{I}_{11\times11}$	$5\mathbf{I}_{11\times11}$
$\mathbf{G}$	$200\mathbf{I}_{6\times6}$	$50\mathbf{I}_{6\times6}$	$50\mathbf{I}_{6\times6}$	$50\mathbf{I}_{6\times6}$
κ	0.4	0.6	0.6	0.01
K_z	0.1	0.1	0.1	10
Z_B	0.1	0.1	0.1	10
g_1	0.5	1	1	1
g_2	1	0.2	0.2	0.2
α_1	1	1	1	1
α_2	0.5	0.5	0.5	0.5
$\bar{\epsilon}$	0.001	0.005	0.005	0.0002

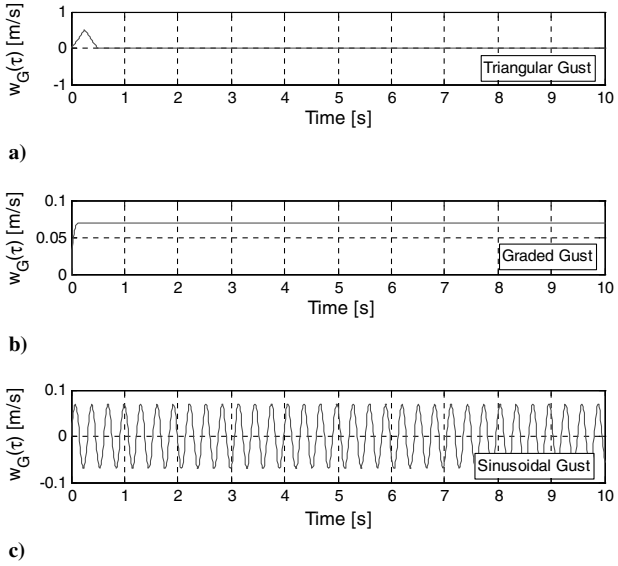

Fig. 2 External disturbances: a) triangular gust; b graded gust; c) sinusoidal gust.

networks compensator and the robustifying term have been defined in Eq. (55) after applying the antiwindup mechanism.

D. Results

In this section, three sets of simulations were run based on three types of external disturbances described above in Eqs. (51–53) then sketched in Fig. 2. The triangular gust disturbance defined in Eq. (51) was the first type of external disturbance considered in the simulation (see Fig. 2a). Figure 3 shows the open-loop response of wing section model at preflutter speed $U_\infty = 8$ [m/s] $< U_F = 11.4$ [m/s] under the triangular gust $w_0 = 0.5$ [m/s] and $w_0 = 0.7$ [m/s], respectively, the errors in the open-loop system settle in about 5 s. In Fig. 4a, one can easily see that the adaptive method in [36] successfully drives the plunge and pitch displacements to zero within 0.5 s when $w_0 = 0.5$ [m/s] and $U_\infty = 8$ [m/s], which is faster than the proposed method (Fig. 4b) in the same condition, since it is a model-based control strategy while our model-free controller needs to learn the unknown model online. Figures 5a and 5b compare the closed-loop response of the system under the triangular gust between the control given in [36] and the proposed controller under a slightly stronger disturbance, namely, $w_0 = 0.7$ [m/s]. As one can see from Fig. 5a, both plunge and pitch displacements keep oscillating and show no sign of convergence by using the method in [36]. However, Fig. 5b shows that the proposed control drives the plunge and pitch

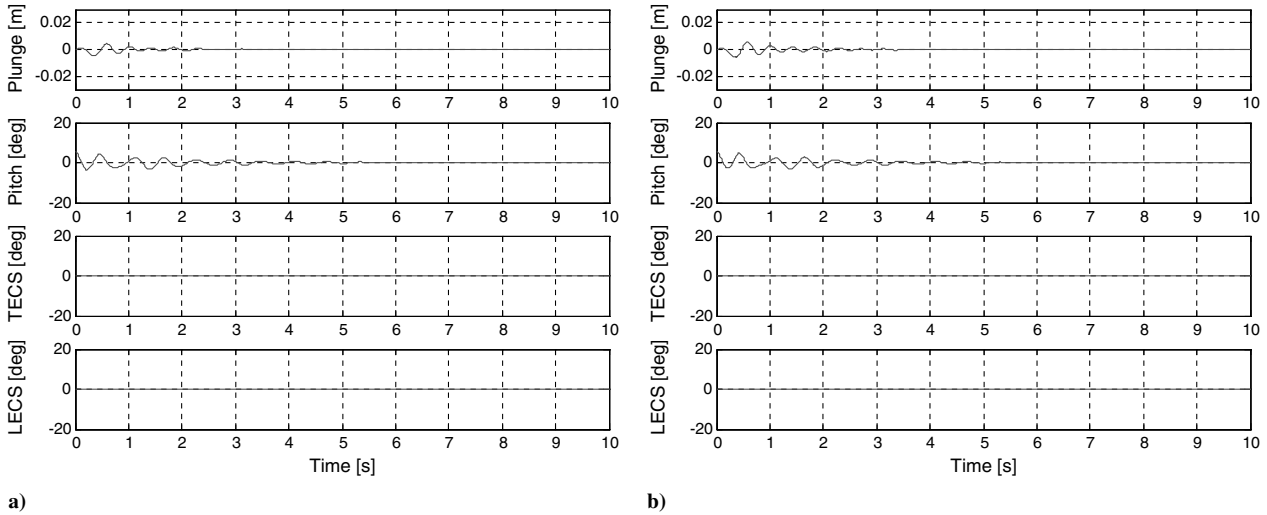

Fig. 3 Open-loop response under triangular gust at preflutter speed $U_\infty = 8$ [m/s]: a) $w_0 = 0.5$ [m/s]; b) $w_0 = 0.7$ [m/s].

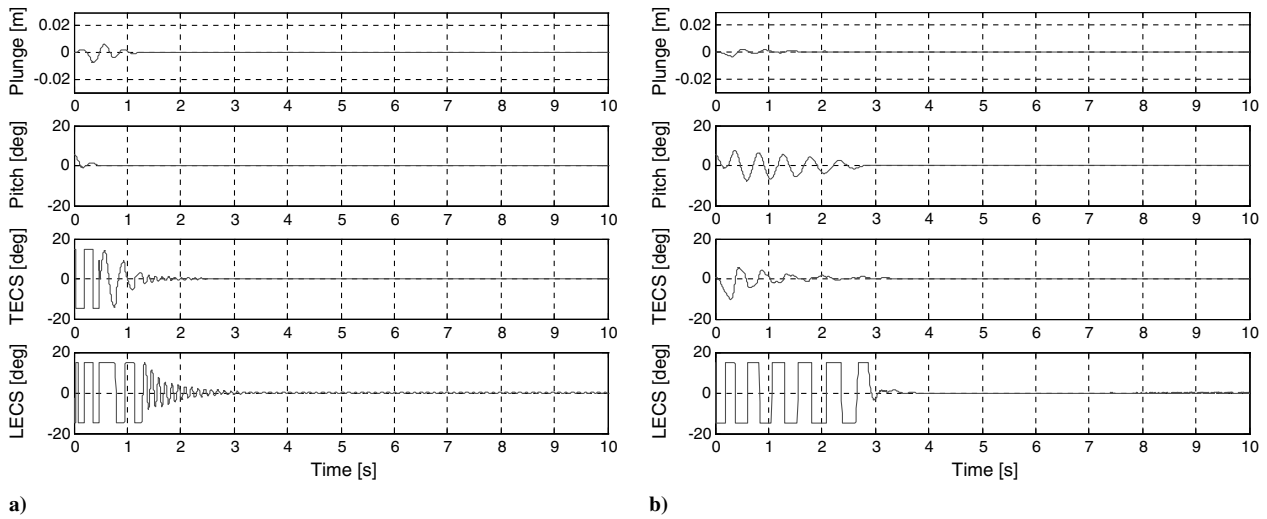

Fig. 4 Closed-loop response under triangular gust $w_0 = 0.5$ [m/s] at preflutter speed $U_\infty = 8$ [m/s]: a) using the method in [36]; b) using the proposed method.

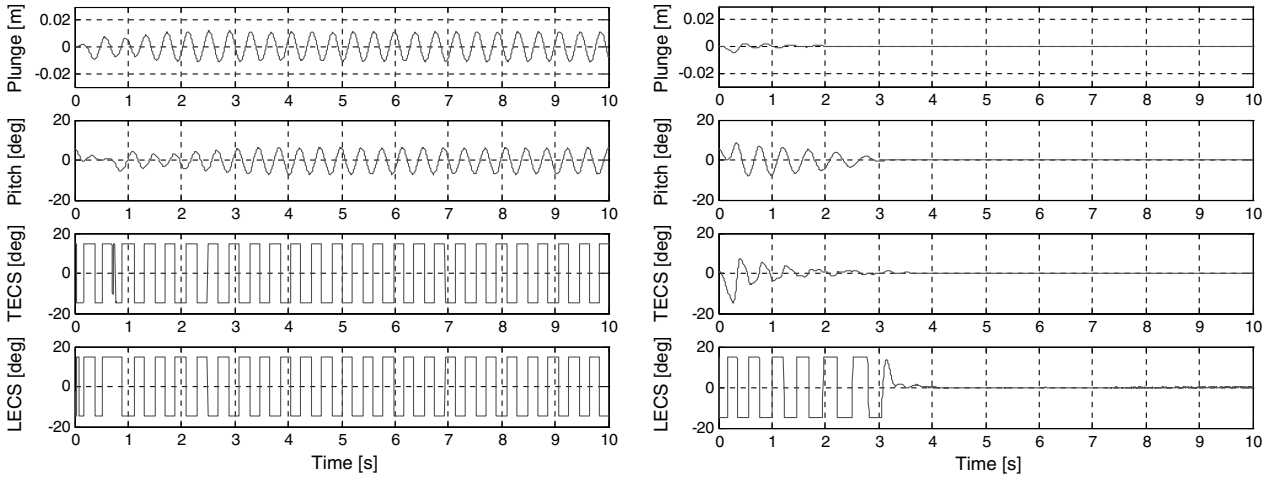

a) b)

Fig. 5 Closed-loop response under triangular gust $w_0 = 0.7$ [m/s] at preflutter speed $U_\infty = 8$ [m/s]: a) using the method in [36]; b) using the proposed method.

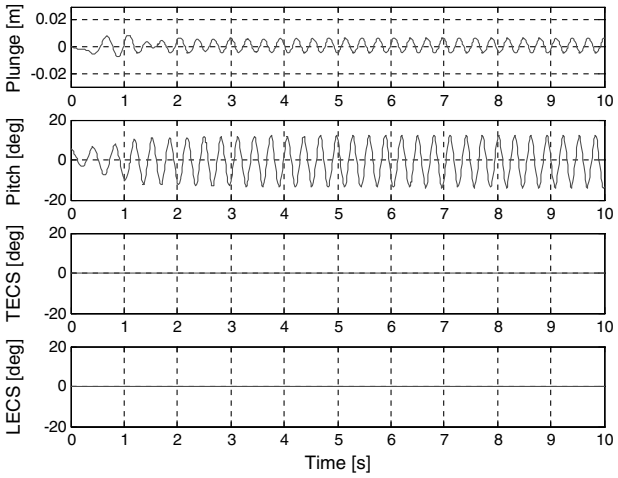

Fig. 6 Open-loop response under triangular gust $w_0 = 0.7$ [m/s] at postflutter speed $U_\infty = 13.28$ [m/s].

displacement to zero in less than 3 s. The oscillatory behavior seen in Fig. 5a stems from the lack of an antiwindup mechanism in [36]. Figure 6 represents the open-loop response of wing section model under the triangular gust $w_0 = 0.7$ [m/s] at postflutter speed $U_\infty = 13.28$ [m/s] $> U_F = 11.4$ [m/s]; it is clear that the system sets into an LCOs. From Figs. 7a and 7b, it can be seen that both the method in [36] as well as the proposed method are able to suppress the LCOs, however, the system settles faster under the proposed control strategy (within 3 s) than it does under the approach proposed in [36] (>5 s).

The open-loop response of the system under graded gust (see Fig. 2b) at postflutter speed $U_\infty = 13.28$ [m/s] $> U_F = 11.4$ [m/s] is given in Fig. 8. In this set of simulations, we first choose a small graded gust $w_0 = 0.07$ [m/s] such that both plunge and pitch displacements are able to converge to zero within the actuator limitations. From Fig. 9, one can easily observe the convergence of the error to the origin under the adaptive method of [36] and the proposed method. Also in this case, the proposed method shows faster settling times. Figure 10 shows the relation between settling time and the control saturation bounds at $U_\infty = 13.28$ [m/s]; here, w_0 is selected as 0.047 [m/s] to ensure that the external disturbance can be compensated by the limited control signals. Here, the control saturation bounds on TECS and LECS have been varied between 10 and 30 deg. It is seen that settling time increases as the saturation bounds are lowered. When we consider a much stronger graded gust,

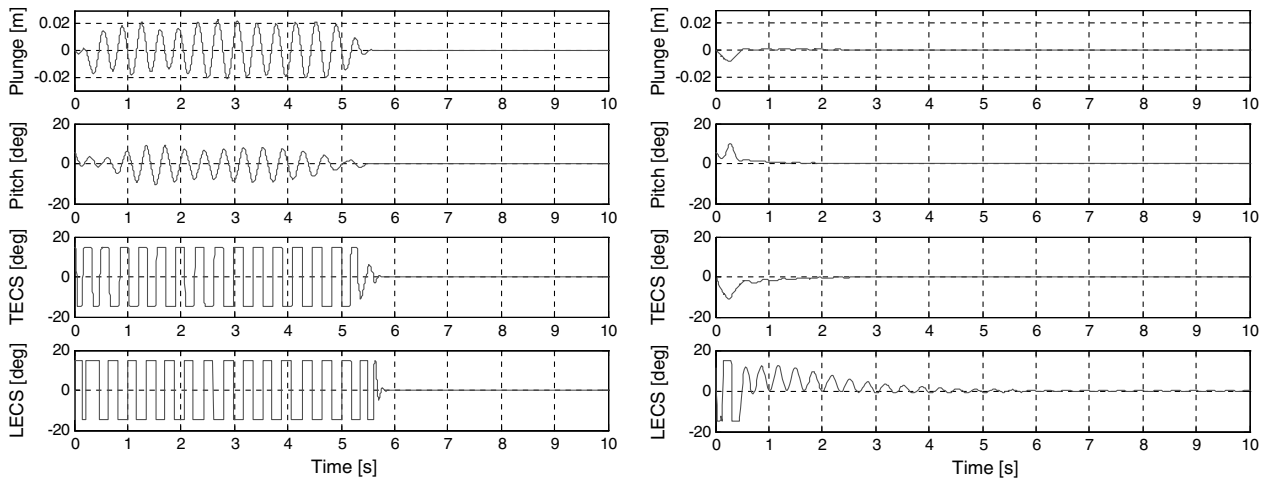

a) b)

Fig. 7 Closed-loop response under triangular gust $w_0 = 0.7$ [m/s] at postflutter speed $U_\infty = 13.28$ [m/s]: a) using the method in [36]; b) using the proposed method.

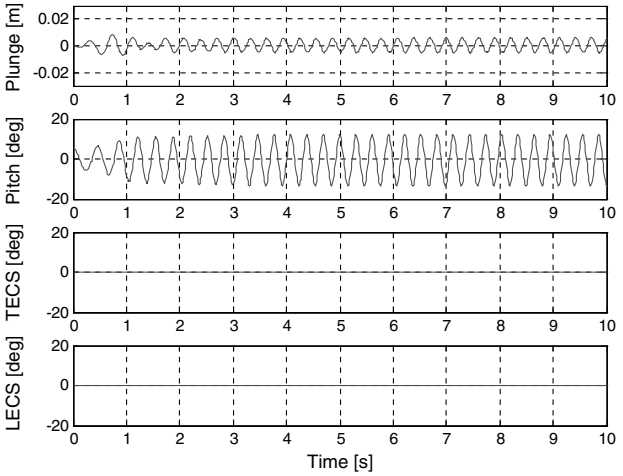

Fig. 8 Open-loop response under graded gust $w_0 = 0.07$ [m/s] at postflutter speed $U_\infty = 13.28$ [m/s].

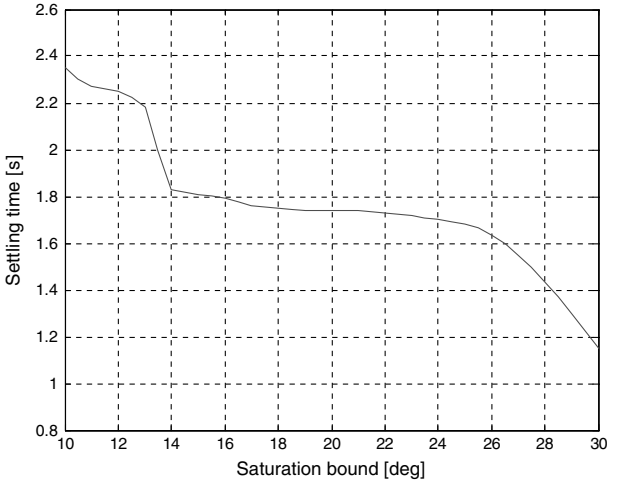

Fig. 10 Relation between the settling time and the control saturation bound on TECS and LECS under graded gust $w_0 = 0.047$ [m/s] at postflutter speed $U_\infty = 13.28$ [m/s].

e.g., $w_0 = 1.0$ [m/s], although the proposed algorithm cannot drive the plunge and pitch displacement to zero due to the limited control energy, however, when compared with the open-loop response seen in Fig. 11, one can still observe the suppression of LCOs from Fig. 12b using the proposed method. Moreover, it is clear from Fig. 12a that the adaptive controller in [36] fails to suppress the LCOs.

Under a sinusoidlike gust (see Fig. 2c) with $w_0 = 0.07$ [m/s] at postflutter speed $U_\infty = 13.28$ [m/s] $> U_F = 11.4$ [m/s], the open-loop response of the system is represented in Fig. 13. Figure 14a shows that the method in [36] needs more than 5 s to stabilize the system. However, the proposed method successfully stabilizes the system in less than 1.5 s. From the LECS control deflection trajectory presented in Fig. 14b, one can clearly see that the control signal is able to compensate for the sinusoidal disturbance injected into the wing section model.

Here we note that since the simulation results under the triangular gust and a more challenging continuous sinusoidal gust are satisfactory, one can expect satisfactory simulation results under other similar disturbances, such as the 1-cosine gust-type disturbance. Generally speaking, the model-free output feedback controller designed in this paper shows substantially greater robustness with respect to modeling uncertainty and various external disturbances as compared with the adaptive backstepping results obtained in [36].

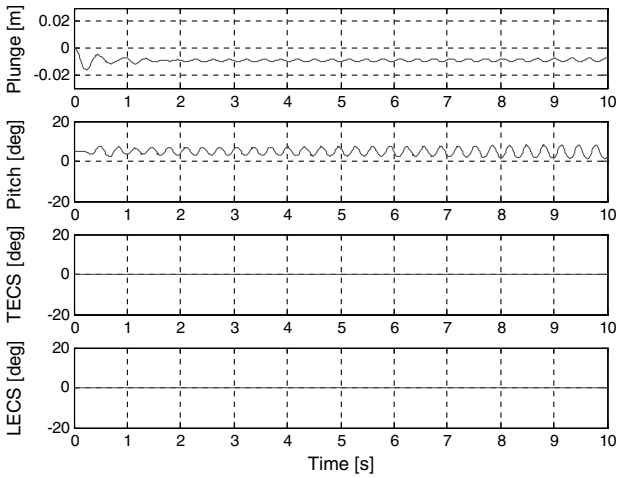

Fig. 11 Open-loop response under graded gust $w_0 = 1.0$ [m/s] at postflutter speed $U_\infty = 13.28$ [m/s].

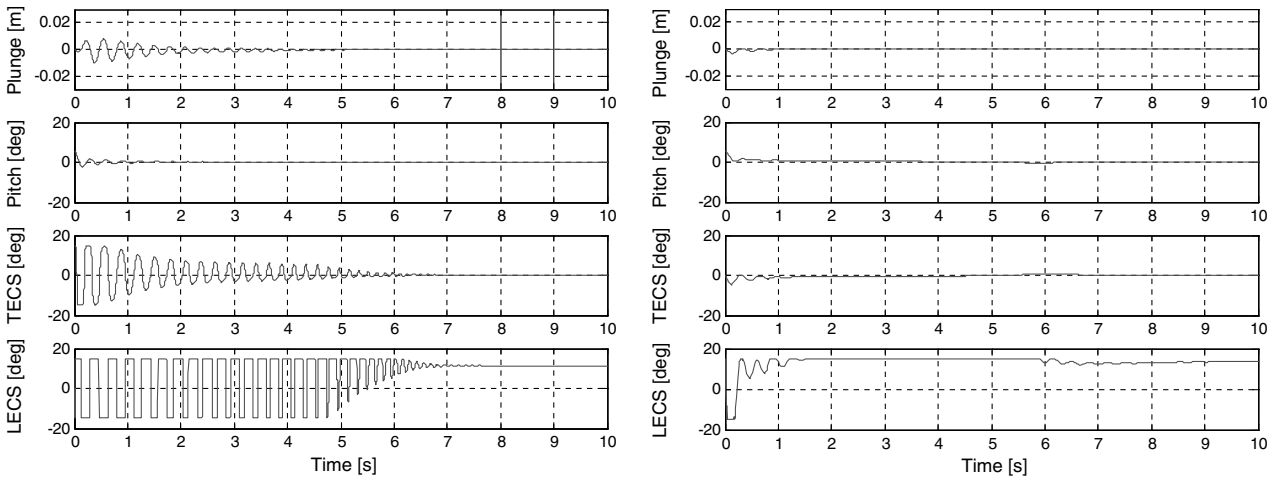

Fig. 9 Closed-loop response under graded gust $w_0 = 0.07$ [m/s] at postflutter speed $U_\infty = 13.28$ [m/s]: a): using the method in [36]; b) using the proposed method.

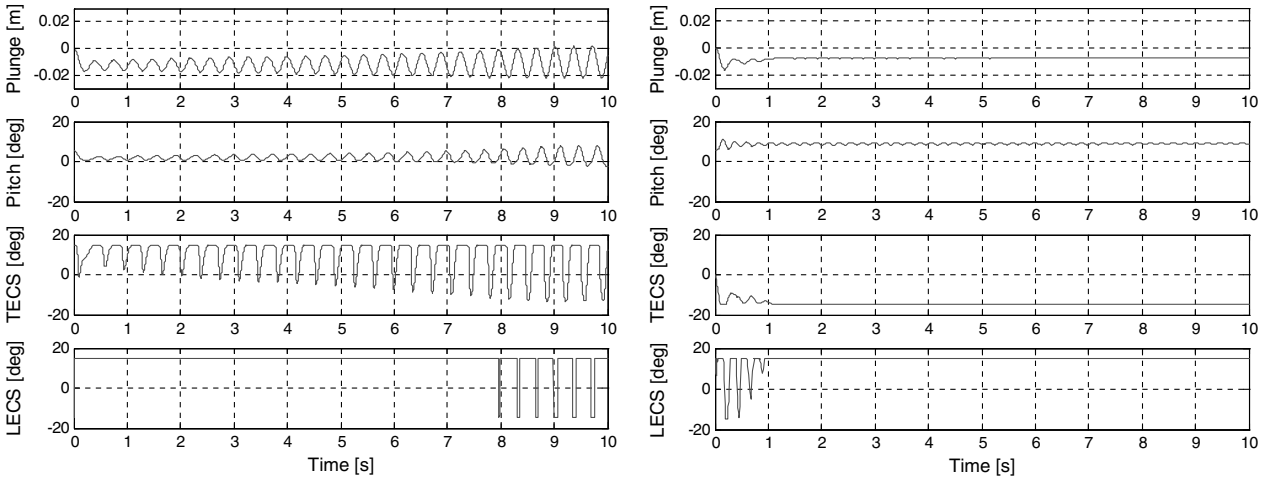

a) b)

Fig. 12 Closed-loop response under graded gust $w_0 = 1.0$ [m/s] at postflutter speed $U_\infty = 13.28$ [m/s]: a) using the method in [36]; b) using the proposed method.

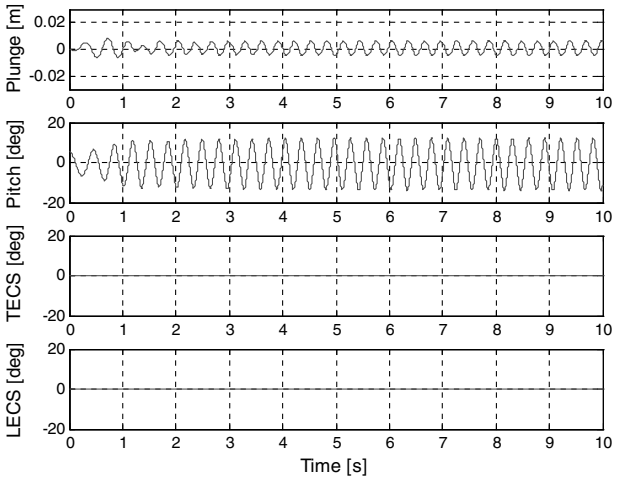

Fig. 13 Open-loop response under sinusoidal gust $w_0 = 0.07$ [m/s] at postflutter speed $U_\infty = 13.28$ [m/s].

VI. Conclusions

In this paper, a modular model-free output feedback controller was proposed to suppress aeroelastic vibrations on unmodeled nonlinear wing section subject to a variety of external disturbances. The control strategy was implemented via leading- γ and trailing-edge β control surfaces. The system structure and parameters, except the signs of the principal minors of the input matrix, were assumed to be unknown in the control design. Compared with traditional adaptive control strategies pursued in [35,36], which strictly require linearity in the model parameters, the proposed method does not require any prior knowledge of the system model. By using a Lyapunov based method for design and analysis, we obtained uniformly ultimately bounded results on the two-axis vibration errors as well as the neural network weight mismatch. High-gain observer was used to design output feedback control when only the output displacements were measurable. In comparison with a backstepping based adaptive output feedback algorithm, simulation results show that the proposed model-free controller more effectively stabilizes pitching and plunging displacements and suppresses the LCOs when subjected to a range of external disturbances. Future work will include the control design for a more complex model of the aeroelastic system, observer implementation under measurement noise, real-time implementation of the neural-network based control, inclusion of actuator dynamics,

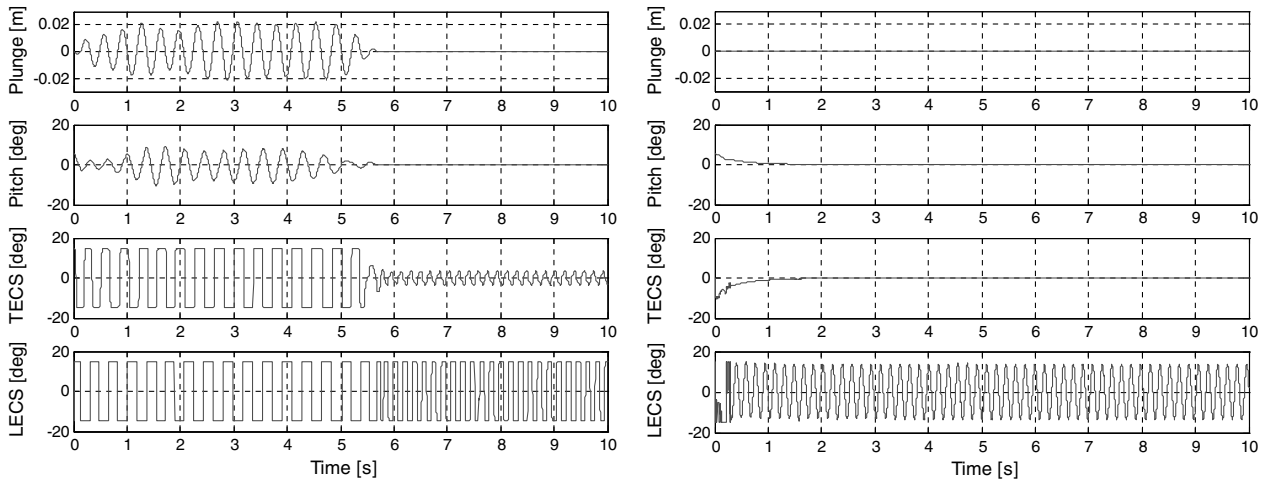

a) b)

Fig. 14 Closed-loop response under sinusoidal gust $w_0 = 0.07$ [m/s] at postflutter speed $U_\infty = 13.28$ [m/s]: a) using the method in [36]; b) using the proposed method.

and experimental evaluation of the model-free controller in the wind-tunnel laboratory at Clarkson University.

References

[1] Librescu, L., and Marzocca, P., "Advances in the Linear/Nonlinear Control of Aeroelastic Structural Systems," *Acta Mechanica*, Vol. 178, Nos. 3–4, Aug. 2005, pp. 147–186. doi:10.1007/s00707-005-0222-6

[2] Noll, T. E., *Flight-Vehicle Materials, Structures, and Dynamics: Assessment and Future Directions*, Vol. 5, American Society of Mechanical Engineering, New York, 1993, pp. 179–212.

[3] Lyons, M. G., Vepa, R., McIntosh, S. C., and DeBra, D. B., "Control Law Synthesis and Sensor Design for Active Flutter Suppression," *Proceedings of the AIAA Guidance and Control Conference*, AIAA Paper 1973-832, 1973.

[4] Mukhopadhyay, V., Newsom, J. R., and Abel, I., "A Direct Method for Synthesizing Low-Order Optimal Feedback Control Laws with Application to Flutter Suppression," *Proceedings of the AIAA Atmospheric Flight Mechanics Conference*, AIAA Paper 1980-1613, 1980.

[5] Gangsaas, D., Ly, U., and Norman, D. C., "Practical Gust Load Alleviation and Flutter Suppression Control Laws Based on LQG Methodology," AIAA Paper 1981-0021, 1981.

[6] Karpel, M., "Design for Active Flutter Suppression and Gust Alleviation Using State-Space Aeroelastic Modeling," *Journal of Aircraft*, Vol. 19, No. 3, 1982, pp. 221–227. doi:10.2514/3.57379

[7] Horikawa, H., and Dowell, E. H., "An Elementary Explanation of the Flutter Mechanism with Active Feedback Controls," *Journal of Aircraft*, Vol. 16, No. 4, 1979, pp. 225–232. doi:10.2514/3.58509

[8] Heeg, J., "Analytical and Experimental Investigation of Flutter Suppression by Piezoelectric Actuation," NASA TP 3241, Sept. 1993.

[9] Lin, C. Y., "Strain Actuated Aeroelastic Control," M.S. Thesis, Department of Aeronautics and Astronautics, Massachusetts Inst. of Technology, Cambridge, MA, Feb. 1993.

[10] Lazarus, K., "Multivariable High-Authority Control of Plate-Like Active Lifting Surfaces," Ph.D. Dissertation, Department of Aeronautics and Astronautics, Massachusetts Inst. of Technology, Cambridge, MA, June 1992.

[11] E. H. Dowell (ed.), Clark, R., Cox, D., Curtiss, H. C., Jr., Edwards, J. W., Hall, K. C., Peters, D. A., Scanlan, R., Simiu, E., Sisto, F., and Strganac, T. W., *A Modern Course In Aeroelasticity*, 4th ed., Kluwer Academic Publisher, Norwell, MA, Jan. 2005.

[12] Breitbach, E., "Effects of Structural Non-Linearities on Aircraft Vibration and Flutter," AGARD Rept. No. 665, Jan. 1978.

[13] Yang, Z. C., and Zhao, L. C., "Analysis of Limit Cycle Flutter of an Airfoil in Incompressible Flow," *Journal of Sound and Vibration,*, Vol. 123, No. 1, 1988, pp. 1–13. doi:10.1016/S0022-460X(88)80073-7

[14] Strganac, T. W., and Mook, D. T., "Numerical Model of Unsteady Subsonic Aeroelastic Behavior," *AIAA Journal*, Vol. 28, No. 5, May 1990, pp. 903–909. doi:10.2514/3.25137

[15] Eastep, F. E., and Olsen, J. J., "Transonic Flutter Analysis of a Rectangular Wing with Conventional Airfoil Sections," *AIAA Journal*, Vol. 18, No. 10, Oct. 1980, pp. 1159–1164. doi:10.2514/3.50866

[16] Edwards, J. W., Bennett, R. M., Whitlow, W., and Seidel, D. A., "Time-Marching Transonic Flutter Solutions Including Angle-of-Attack Effects," *Journal of Aircraft*, Vol. 20, No. 11, Nov. 1983, pp. 899–906. doi:10.2514/3.48190

[17] Mukhopadhyay, V., "Benchmark Active Control Technology," *Journal of Guidance, Control, and Dynamics*, Vol. 23, Nos. 5–6, 2000, pp. 913–960, 1093–1139; also Vol. 24, No. 1, 2001, pp. 146–192. doi:10.2514/2.4631.

[18] Wazak, M., and Srinathkumar, S., "Design and Experimental Validation of a Flutter Suppression Controller for the Active Flexible Wing,"NASA TM 4381, Washington, D.C., 1992.

[19] Mukhopadhyay, V., "Flutter Suppression Digital Control Law Design and Testing for the AFW Wind Tunnel Model," NASA TM 107652, Hampton, VA, 1992.

[20] Ko, J., Kurdila, A. J., and Strganac, T. W., "Nonlinear Control of a Prototypical Wing Section with Torsional Nonlinearity," *Journal of Guidance, Control, and Dynamics*, Vol. 20, No. 6, 1997, pp. 1181–1189. doi:10.2514/2.4174

[21] Vipperman, J. S., Clark, R. L., Conner, M. D., and Dowell, E. H., "Investigation of the experimental active control of a typical section airfoil using a trailing edge flap," *Journal of Aircraft*, Vol. 35, No. 2, 1998, pp. 224–229. doi:10.2514/2.2312

[22] Ko, J., Strganac, T. W., and Kurdila, A. J., "Stability and Control of Structurally Nonlinear Aeroelastic System," *Journal of Guidance, Control, and Dynamics*, Vol. 21, No. 5, 1998, pp. 718–725. doi:10.2514/2.4317

[23] Ko, J., Strganac, T. W., and Kurdila, A. J., "Adaptive Feedback Linearization for the Control of a Typical Wing Section With Structural Nonlinearity," *Nonlinear Dynamics*, Vol. 18, No. 3, 1999, pp. 289–301. doi:10.1023/A:1008323629064

[24] Strganac, T. W., Ko, J., and Thompson, D. E., "Identification and Control of Limit Cycle Oscillations in Aeroelastic Systems," *Journal of Guidance, Control, and Dynamics*, Vol. 23, No. 6, 2000, pp. 1127–1133. doi:10.2514/2.4664

[25] Xing, W., and Singh, S. N., "Adaptive Output Feedback Control of a Nonlinear Aeroelastic Structure," *Journal of Guidance, Control, and Dynamics*, Vol. 23, No. 6, 2000, pp. 1109–1116. doi:10.2514/2.4662

[26] Strganac, T. W., Ko, J., and Thompson, D. E., "Identification and Control of Limit-Cycle Oscillations in Aeroelastic Systems," *Journal of Guidance, Control, and Dynamics*, Vol. 23, No. 6, 2000, pp. 1127–1133. doi:10.2514/2.4664

[27] Zhang, R., and Singh, S. N., "Adaptive Output Feedback Control of an Aeroelastic System with Unstructured Uncertainties," *Journal of Guidance, Control, and Dynamics*, Vol. 24, No. 3, 2001, pp. 502–509. doi:10.2514/2.4739

[28] Singh, S. N., and Wang, L., "Output Feedback Form and Adaptive Stabilization of a Nonlinear Aeroelastic System," *Journal of Guidance, Control, and Dynamics*, Vol. 25, No. 4, 2002, pp. 725–732. doi:10.2514/2.4939

[29] Behal, A., Marzocca, P., Rao, V. M., and Gnann, A., "Nonlinear Adaptive Control of an Aeroelastic Two-Dimensional Lifting Surface," *Journal of Guidance, Control, and Dynamics*, Vol. 29, No. 2, 2006, pp. 382–390. doi:10.2514/1.14011

[30] Lee, K. W., and Singh, S. N., "Global Robust Control of an Aeroelastic System Using Output Feedback," *Journal of Guidance, Control, and Dynamics*, Vol. 30, No. 1, 2007, pp. 271–275. doi:10.2514/1.22940

[31] Zhang, F., and Soffker, D., "Active Flutter Suppression of a Nonlinear Aeroelastic System Using PI-Observer," *Motion and Vibration Control*, edited by H. Ulbrich, L. Ginzinger, Springer, The Netherlands, 2009, pp. 367–376.

[32] Lee, K. W., and Singh, S. N., "Immersion and Invariance Based Adaptive Control of a Nonlinear Aeroelastic System," *Journal of Guidance, Control, and Dynamics*, Vol. 32, No. 4, 2009, pp. 1100–1110. doi:10.2514/1.42475

[33] Platanitis, G., and Strganac, T. W., "Control of a Nonlinear Wing Section Using Leading- and Trailing-Edge Surfaces," *Journal of Guidance, Control, and Dynamics*, Vol. 27, No. 1, 2004, pp. 52–58. doi:10.2514/1.9284

[34] Gujjula, S., Singh, S. N., and Yim, W., "Adaptive and Neural Control of a Wing Section Using Leading- and Trailing-Edge Surfaces," *Aerospace Science and Technology*, Vol. 9, No. 2, 2005, pp. 161–171. doi:10.1016/j.ast.2004.10.003

[35] Behal, A., Rao, V. M., Marzocca, P., and Kamaludeen, M., "Adaptive Control for a Nonlinear Wing Section with Multiple Flaps," *Journal of Guidance, Control, and Dynamics*, Vol. 29, No. 3, 2006, pp. 744–749. doi:10.2514/1.18182

[36] Reddy, K. K., Chen, J., Behal, A., and Marzocca, P., "Multi-Input/Multi-Output Adaptive Output Feedback Control Design for Aeroelastic Vibration Suppression," *Journal of Guidance, Control, and Dynamics*, Vol. 30, No. 4, 2007, pp. 1040–1048. doi:10.2514/1.27684

[37] Tao, G., *Adaptive Control Design and Analysis*, Wiley, New York, 2003, pp. 458–472.

[38] Marzocca, P., Librescu, L., and Chiocchia, G., "Aeroelastic Response of 2-D Lifting Surfaces to Gust and Arbitrary Explosive Loading Signatures," *International Journal of Impact Engineering*, Vol. 25, No. 1, 2001, pp. 41–65. doi:10.1016/S0734-743X(00)00033-6

[39] Block, J. J., and Strganac, T. W., "Applied Active Control for a Nonlinear Aeroelastic Structure," *Journal of Guidance, Control, and Dynamics*, Vol. 21, No. 6, 1998, pp. 838–845.

doi:10.2514/2.4346

[40] Chen, J., Behal, A., and Dawson, D. M., "Robust Feedback Control for a Class of Uncertain MIMO Nonlinear Systems," *IEEE Transactions on Automatic Control*, Vol. 53, No. 2, March 2008, pp. 591–596. doi:10.1109/TAC.2008.916658

[41] Morse, A. S., "A Gain Matrix Decomposition and Some of its Applications," *Systems and Control Letters*, Vol. 21, No. 1, 1993, pp. 1–10. doi:10.1016/0167-6911(93)90038-8

[42] Lewis, F. L., Dawson, D. M., and Abdallah, C. T., *Robot Manipulator Control: Theory and Practice*, 2nd ed., CRC Press, Boca Raton, FL, 2003.

[43] Khalil, H., *Nonlinear Systems*, Prentice-Hall, Upper Saddle River, NJ, 1996.

[44] Lewis, F. L., Abdallah, C. T., and Dawson, D. M., *Control of Robot Manipulator*, Macmillam, New York, 1993.

[45] Atassi, A. N., and Khalil, H., "A Separation Principle for the Stabilization of a Class of Nonlinear Systems," *IEEE Transactions on Automatic Control*, Vol. 44, No. 9, Sept. 1999, pp. 1672–1687. doi:10.1109/9.788534

[46] Ahrens, J. H., and Khalil, H. K., "High-Gain Observers in the Presence of Measurement Noise: A Switched Gain Approach," *Automatica*, Vol. 45, No. 4, 2009, pp. 963–943.

[47] Vasiljevica, L. K., and Khalil, H. K., "Error Bounds in Differentiation of Noisy Signals by High-Gain Observers," *Systems and Control Letters*, Vol. 57, No. 10, Oct. 2008, pp. 856–862. doi:10.1016/j.sysconle.2008.03.018

[48] Åström, K. J., and Rundqwist, L., "Integrator Windup and How to Avoid It," *Proceedings of the American Control Conference*, IEEE Publications, Piscataway, NJ, 1989, pp. 1693–1698.